Total character count: 49,903 including spaces

Title: The yeast mitochondrial pyruvate carrier is a hetero-dimer in its functional state

Authors: Sotiria Tavoulari[1*], Chancievan Thangaratnarajah[1†], Vasiliki Mavridou[1], Michael E. Harbour[1], Jean-Claude Martinou[2] and Edmund R.S. Kunji[1*]

Institutions:

[1]Medical Research Council Mitochondrial Biology Unit, University of Cambridge, Wellcome Trust/MRC Building, Cambridge Biomedical Campus, Hills Road, Cambridge, CB2 0XY United Kingdom.

[2]Department of Cell Biology, University of Geneva, 30 Quai Ernest-Ansermet, 1211 Genève 4, Switzerland

†Current address: Groningen Biomolecular Sciences and Biotechnology Institute, Membrane Enzymology, University of Groningen, Nijenborgh 4, 9747 AG, Groningen, The Netherlands.

***Corresponding authors**:

Sotiria Tavoulari, Medical Research Council Mitochondrial Biology Unit, University of Cambridge, Wellcome Trust/MRC Building, Cambridge Biomedical Campus, Hills Road, Cambridge, CB2 0XY United Kingdom, Tel: +441223252850, Fax: +441223252875, Email: st632@mrc-mbu.cam.ac.uk

Edmund R.S. Kunji, Medical Research Council Mitochondrial Biology Unit, University of Cambridge, Wellcome Trust/MRC Building, Cambridge Biomedical Campus, Hills Road, Cambridge, CB2 0XY United Kingdom, Tel: +441223252850, Fax: +441223252875, Email: ek@mrc-mbu.cam.ac.uk

Running title: The functional unit of MPC

Abstract (175 words)

The mitochondrial pyruvate carrier (MPC) is critical for cellular homeostasis, as it is required in central metabolism for transporting pyruvate from the cytosol into the mitochondrial matrix. MPC has been implicated in many diseases and is being investigated as a drug target. A few years ago, small membrane proteins, called MPC1 and MPC2 in mammals and Mpc1, Mpc2 and Mpc3 in yeast, were proposed to form large protein complexes responsible for this function. However, the MPC complexes have never been isolated and their composition, oligomeric state and functional properties have not been defined. Here, we identify the functional unit of MPC from *Saccharomyces cerevisiae*. In contrast to earlier hypotheses, we demonstrate that MPC is a hetero-dimer, not a multimeric complex. When not engaged in hetero-dimers, the yeast Mpc proteins can also form homo-dimers that are, however, inactive. We show that the earlier described substrate transport properties and inhibitor profiles are embodied by the hetero-dimer. This work provides a foundation for elucidating the structure of the functional complex and the mechanism of substrate transport and inhibition.

Key words: mitochondria / oligomeric state / pyruvate / protein complex / transport proteins

Introduction

In recent years, there is an increasing understanding and appreciation that mitochondrial metabolism is involved in major human diseases, such as cancer, neurodegeneration, cardiovascular diseases, metabolic disorders, obesity and diabetes. A key player for the metabolic fate of the cell is the mitochondrial pyruvate carrier (MPC), a protein responsible for the uptake of pyruvate from the cytosol into the mitochondrial matrix (Vanderperre et al., 2015), where it enters the tricarboxylic acid cycle and other biosynthetic pathways. The existence of a membrane protein responsible for pyruvate transport across the mitochondrial inner membrane had been supported by early work on isolated mitochondria, where pyruvate transport had been shown to be saturating and pH-dependent (Papa et al., 1971, Papa & Paradies, 1974). In addition, small molecule inhibitors had been identified in support of this notion (Halestrap, 1975, Halestrap, 1976, Halestrap & Denton, 1974), but the molecular identity of the protein remained unknown for four decades.

Major progress was made in 2012, when mitochondrial pyruvate transport activity was discovered to be associated with two small homologous proteins, MPC1 and MPC2 (Bricker et al., 2012, Herzig et al., 2012). In mammals and drosophila the expression of both MPC proteins is necessary for pyruvate transport (Bricker et al., 2012, Herzig et al., 2012). In yeast *Saccharomyces cerevisiae*, three proteins Mpc1, Mpc2 and Mpc3 are expressed in a carbon source-dependent pattern, forming an Mpc1/Mpc2 complex under fermentative conditions and an Mpc1/Mpc3 under respiratory conditions, called MPC_{FERM} and MPC_{OX} complexes, respectively (Bender et al., 2015, Compan et al., 2015).

As the mitochondrial pyruvate carrier is central for cellular homeostasis, the identification of the MPC proteins intensified efforts to understand their role in cancer (Bader et al., 2019, Corbet et al., 2018, Li et al., 2017, Li et al., 2016, Ohashi et al., 2018, Schell et al., 2014, Schell et al., 2017, Yang et al., 2014, Zhong et al., 2015), diabetes (Colca et al., 2013, Divakaruni et al., 2013, Gray et al., 2015, McCommis et al., 2015, McCommis et al., 2016, Vadvalkar et al., 2017, Vigueira et al., 2014) and neurodegeneration (Divakaruni et al., 2017, Ghosh et al., 2016, Quansah et al., 2018). Moreover, pathogenic mutations in the *mpc1* gene were found in rare but severe metabolic syndromes, further enhancing the clinical relevance of this transporter (Bricker et al., 2012). Additionally, an increasing number of small-

molecule drugs, previously known to have other targets, have now been proposed to inhibit MPC activity (Chen et al., 2018, Colca et al., 2013, Corbet et al., 2018, Divakaruni et al., 2013, Du et al., 2013, Ghosh et al., 2016, Nancolas et al., 2016, Nath et al., 2016). MPC is a newly identified target for the first generation insulin sensitisers, called thiazolidinediones (TZDs) (Colca et al., 2013, Divakaruni et al., 2013), originally known to exert their action on the peroxisome proliferator-activated receptor gamma (PPARγ) (Nanjan et al., 2018, Soccio et al., 2014). More recently, a new generation TZD, bypassing PPARγ (Colca et al., 2014) and currently in clinical trials for the treatment of Parkinson's disease, was proposed to exert its action by inhibiting MPC (Ghosh et al., 2016). Despite these major advances, a direct experimental system to measure the interactions of small-molecule drugs with MPC and to study the mechanism of inhibition is not available.

Six years after the primary identification of the MPC proteins (Bricker et al., 2012, Herzig et al., 2012), there has been no report of a successful purification and functional reconstitution of an MPC hetero-complex. Consequently, the composition of the MPC complexes, the oligomeric state and the protomer stoichiometry remain controversial (Bender et al., 2015, Bricker et al., 2012, Nagampalli et al., 2018) and their involvement in pyruvate transport has been questioned (Halestrap, 2012). The yeast MPC hetero-complexes migrate at 150 kDa (Bender et al., 2015, Bricker et al., 2012) or at even higher molecular weights (Bender et al., 2015) in blue native gel electrophoresis, leading to proposals that the complexes are multimeric and might even include additional, yet unidentified proteins (Bricker et al., 2012, Halestrap, 2012). The application of chemical cross-linking on MPC proteins has produced bands corresponding to monomers, dimers as well as higher oligomers (Bender et al., 2015, Nagampalli et al., 2018). In the only published attempt to purify an MPC hetero-complex, it was only possible to purify individual MPC protomers (Nagampalli et al., 2018). It has also been proposed that the individual human MPC2 protein can form high-order multi-species capable of transporting pyruvate (Nagampalli et al., 2018), raising more questions regarding the functional unit of the mitochondrial pyruvate carrier.

Here, we report the first successful purification and characterisation of MPC hetero-complexes from yeast, providing a model system for future structural and mechanistic studies. We demonstrate that the natural state of yeast MPC is a hetero-

dimer capable of transporting pyruvate. In the absence of other protomers, MPC proteins can form homo-dimers, but they do not transport pyruvate.

Results

Expression and purification of the yeast Mpc proteins

Although it has been established that the MPC proteins constitute the mitochondrial pyruvate carrier (Bricker et al., 2012, Herzig et al., 2012), there are still many outstanding questions regarding the composition and the oligomeric state of the functional complex. The most straightforward way to settle these issues is through the purification and reconstitution of the individual components and putative complexes to determine whether they have pyruvate transport activity.

Here, we have used the Mpc proteins from *S. cerevisiae* (Fig EV1) as a model system to study the composition and functional properties of the mitochondrial pyruvate carrier. We decided to concentrate on the Mpc1/Mpc3 complex, as it is the principle pyruvate carrier in oxidative phosphorylation (MPC_{OX}) (Bender et al., 2015). It is also the most related to MPCs of mammals and other organisms, whereas the Mpc1/Mpc2 complex (MPC_{FERM}), expressed under fermentative conditions, only exists in some fungi. The principal approach was to purify the Mpc1/Mpc3 hetero-complex by tagging one of the two protomers with a Factor Xa cleavage site and an eight-histidine tag on the C-terminus (Fig 1A). To achieve co-expression of the protein pair we used an inducible bi-directional vector (Miller et al., 1998) for expression in mitochondria of the *mpc* triple deletion strain SHY15 (Herzig et al., 2012). We also expressed the C-terminally tagged Mpc1 and Mpc3 proteins individually in yeast mitochondria.

All proteins expressed well, both in the presence and the absence of their proposed complex partner (Fig 1B). It is notable though that in expression trials of Mpc1 alone an additional prominent band appeared, approximately corresponding to the molecular weight of an SDS-resistant dimer, as detected by immunoblotting of crude yeast mitochondrial preparations (Fig 1B, left panel). However, this band was not detected in mitochondria expressing the untagged Mpc1 protein (Fig 1B, left panel). For these reasons, we chose to co-express an unmodified Mpc1 together with a tagged Mpc3 for hetero-complex formation.

With this strategy, the purification of the Mpc1/Mpc3 hetero-complex was successful and both proteins were present in a 1:1 ratio (Fig 1C). The highest protein

yield (~1 mg protein per g of mitochondria) was achieved with the detergent lauryl maltose neopentyl glycol (LMNG), supplemented with tetraoleoyl cardiolipin. However, the stoichiometric Mpc1/Mpc3 complex could also be purified in Triton X-100, decyl maltose neopentyl glycol (DMNG) or *n*-dodecyl β-D-maltoside (DDM), each supplemented with tetraoleoyl cardiolipin, albeit with lower purification yields (Fig EV2). In LMNG and tetraoleoyl cardiolipin, the Mpc1/Mpc3 complex eluted as a single peak by size-exclusion chromatography, indicating that the complex was monodisperse (Fig EV3). Moreover, analysis of the peak fractions showed that the protomers remained associated during purification, consistent with a stable complex (Fig EV3, A, inset). When we purified histidine-tagged Mpc1 or Mpc3 on their own in LMNG and tetraoleoyl cardiolipin (Fig 1C), the yields were at least three times lower, despite similar expression levels in mitochondria in the presence or absence of their partner (Fig 1B), indicating stability issues. After purification and histidine-tag cleavage, Mpc1 contained again an SDS-resistant dimer (Fig 1C), as detected by peptide mass fingerprinting (Table EV1).

Next, we used thermostability analysis to evaluate folding and stability of the hetero-complex and its components. For this purpose, we monitored the unfolding of protein populations in a temperature ramp in the presence of 7-diethylamino-3-(4-maleimidophenyl)-4-methylcoumarin (CPM), which reacts with cysteine residues becoming exposed due to denaturation (Fig 1D). Mpc1 and Mpc3 both have a single cysteine residue (Fig EV1). The Mpc1/Mpc3 hetero-complex and the individual Mpc3 protein had very similar unfolding profiles and melting temperatures (52.0 and 51.7 °C respectively), clearly showing that they are folded and stable in detergent solution. The Mpc1 protein on its own, however, did not display a thermal denaturation profile and high fluorescence was detected throughout the temperature ramp. This result means that either Mpc1 is unfolded or its single cysteine is already exposed. To discriminate between these two possibilities, we also performed thermostability analysis by nano differential scanning fluorimetry (nanoDSF) (Fig 1E), which relies on changes in the environment of endogenous tyrosine and tryptophan residues. Again, the hetero-complex and Mpc3 had similar apparent melting temperatures, 48.5 and 48.0 °C, respectively, similar to those obtained with CPM. However, Mpc1 alone showed a peak at 64.5 °C, which might correspond to the SDS-resistant dimer, possibly being an aggregation artefact.

The ability of Mpc proteins to form hetero-complexes was also demonstrated when we expressed and purified the Mpc1/Mpc2 (MPC_{FERM}) hetero-complex (Bender et al., 2015) using a histidine tag on Mpc2 (Fig EV4, A and B). We also compared the Mpc1/Mpc2 hetero-complex to the histidine-tagged Mpc2, expressed and purified alone (Fig EV4). Although Mpc2 can be expressed in mitochondria equally well on its own or together with Mpc1 (Fig EV4, A), it could not be purified alone in sufficient quantities and could only be detected by peptide mass fingerprinting (Fig EV4, B and Table EV1). Interestingly though, when they were expressed together, Mpc2 with Mpc1 successfully formed a hetero-complex, which was purified and had an apparent melting temperature of 42 °C (Fig EV4, C).

This is the first purification of MPC hetero-complexes, demonstrating that different Mpc protomers can form stable interactions. Of the two hetero-complexes, the principal complex Mpc1/Mpc3 was purified at higher yields, was 10°C more thermostable and was, therefore, selected for characterisation of its oligomeric state.

The Mpc1/Mpc3 hetero-complex is a dimer.

We showed that the protomers are present in a 1:1 molar ratio in the hetero-complexes (Fig 1C), but this does not resolve the issue of the overall mass of the complex. Previous work on the yeast Mpc proposed that the protein is a multimeric complex of 150 kDa, based on its electrophoretic mobility by blue native gel electrophoresis (Bricker et al., 2012) and this notion has been largely accepted in the literature. However, the electrophoretic mobility on blue native gels depends on the associated detergent and lipids present during protein extraction, as both the detergent-lipid micelle (DL) and the protein bind Coomassie stain, leading to anomalous migration (Crichton et al., 2013). Therefore, blue native gel electrophoresis is not an appropriate technique for sizing of small membrane proteins. Another approach that has been used involves chemical cross-linking with 7 and 15 Å long cross-linkers. The cross-linked MPC proteins appeared on SDS-PAGE in multiple bands corresponding to monomers, dimers and different higher oligomers (Bender et al., 2015, Nagampalli et al., 2018), but it cannot be excluded that the detected states are the result of non-specific cross-linking events.

Here, we determined the molecular mass, oligomeric state and subunit stoichiometry of the affinity-purified Mpc1/Mpc3 hetero-complex by using size-

exclusion chromatography linked to multi-angle laser light scattering (SEC-MALLS) (Figs 2A and B). This technique can determine the mass of the protein-detergent-lipid complex (PDL) and of the protein itself (Slotboom et al., 2008, ter Beek et al., 2011). The analysis showed that on average the mass of the Mpc1/Mpc3 hetero-complex is contributing 30.8 ± 1.4 kDa to a 163.3 ± 5.1 kDa protein-detergent-lipid complex (Table EV2 and Fig 2B). The protein mass corresponded well to the sum of the theoretical masses of Mpc1 (15 kDa) and Mpc3 (17.1 kDa), which demonstrates that the complex is a hetero-dimer. Similar results were obtained whether the protein was purified by a single affinity chromatography step or by an additional size-exclusion chromatography step (Table EV2).

To exclude other possible stoichiometries, we performed an internal consistency analysis (Wen et al., 1996), where theoretical molecular masses for the complex, corresponding to different possible subunit stoichiometries, were calculated and compared with the experimentally determined molecular mass. The analysis was only consistent with a Mpc1/Mpc3 hetero-dimeric complex, showing the smallest difference between the experimentally determined and theoretical molecular masses (Table 1). Additionally, since Mpc1 and Mpc3 co-purify in equimolar amounts and remain associated throughout the SEC-MALLS step (Fig 2B, inset), the possibility that the calculated mass corresponds to separate homo-dimers is eliminated.

Since Mpc3 can be purified on its own (Figs 1C and EV3) and is stable in solution, it was also analysed by SEC-MALLS (Fig 2C and D). The average molecular mass for the protein-detergent-lipid complex was 182.9 ± 7.9 kDa with the protein contributing 34.8 ± 0.7 kDa (Table EV2 and Fig 2D), which is approximately twice the theoretical mass of Mpc3 (17.1 kDa). Thus, Mpc3 forms homo-dimers in the absence of Mpc1.

The Mpc1/Mpc3 hetero-dimer is the active mitochondrial pyruvate carrier

To investigate whether the Mpc1/Mpc3 hetero-dimer is capable of pyruvate transport, we established a reconstitution and transport protocol. We prepared proteoliposomes of the purified hetero-dimer loaded with 5 mM unlabelled pyruvate in buffer at pH 8.0 (Fig 3) or 7.4 (Fig EV5) and we initiated pyruvate homo-exchange by addition of radiolabelled pyruvate (50 µM) on the outside. To evaluate the pH dependence of transport, we performed our assays with external buffer at different pH units (Fig 3 and EV5).

In proteoliposomes loaded with internal buffer at pH of 7.4 (Fig EV5) we observed that diffusion, as determined by [^{14}C]-pyruvate accumulation in empty liposomes, was pH-dependent and highest in acidic pH of 5.4, when pyruvate accumulation into empty liposomes reached levels even higher than into proteoliposomes. This result is consistent with previous studies suggesting that pyruvate can cross the mitochondrial membrane via “absorption”, depending on its protonation state (Bakker & van Dam, 1974, Klingenberg, 1970, Zahlten et al., 1972). Therefore, the selection of internal and external pH units is critical. Our finalised pyruvate transport protocol (Fig 3) was based on achieving the maximal ΔpH under conditions where the diffusion is minimal.

When we selected an internal pH of 8.0 and external pH of 6.4, yielding a ΔpH of 1.6, high pyruvate homo-exchange activity was observed (Fig 3A) with an initial uptake rate of 1.6 ± 0.2 μmol/min/mg protein, demonstrating that the purified Mpc1/Mpc3 hetero-dimer is capable of transporting pyruvate. This homo-exchange reaction was completed within seconds when performed at room temperature. Under these conditions, the maximum transport rate (V_{max}) was 8 ± 3 μmol/min/mg protein and the apparent K_M of transport for pyruvate was 342 ± 58 μM (Fig 3B). We were also able to measure homo-exchange activity at a ΔpH of 0.8 (internal pH of 8.0, external pH of 7.2), which is physiologically relevant to mitochondria, albeit with lower signal (Fig 3C). The activity was abolished in the absence of a ΔpH (Fig 3D), showing that transport is pH-dependent, as previously proposed for the carrier in mitochondria (Papa et al., 1971, Papa & Paradies, 1974). Importantly, the Mpc1/Mpc2 hetero-complex was also active for ΔpH-dependent pyruvate transport (Figure EV4, D).

It is expected that transport by a functional MPC should be inhibited by UK5099, a well-established inhibitor of pyruvate transport in rat, mouse or human mitochondria (Halestrap, 1975). We tested whether UK5099 can also inhibit pyruvate homo-exchange by the yeast Mpc1/Mpc3 hetero-dimer. Indeed, in the presence of UK5099 the initial rates of transport were inhibited, with the IC_{50} being at the low micromolar range (9 ± 7 μM from three biological repeats and Fig 3E). This is a greater value than reported for mammalian MPC proteins, where the IC_{50} for UK5099 is in the nanomolar range, probably reflecting differences in inhibitor binding between yeast and mammalian complexes. We also tested Zaprinast, a phosphodiesterase inhibitor, which was reported to block pyruvate oxidation and pyruvate influx in

mouse mitochondria (Du et al., 2013), and 7ACC2, a carboxycoumarin inhibitor of the monocarboxylate transporter 1 (MCT1), also proposed to inhibit MPC. The inhibition of pyruvate exchange was similar for Zaprinast and 7ACC2 with an average IC_{50} of 18 ± 8 μM and 27 ± 13 μM, respectively. Lonidamine, an anti-tumour agent proposed to inhibit the monocarboxylate transporters (MCTs) as well as MPC, inhibited the yeast hetero-complex but with a higher IC_{50} of 118 ± 24 μM. Finally, we tested two thiazolidinediones (Fig 3F). Unlike the other tested compounds, pioglitazone had no effect on pyruvate transport by Mpc1/Mpc3. Rosiglitazone inhibited pyruvate transport to 52 ± 7 % but at a high concentration (500 μM) suggesting that some TZDs might be inhibiting the yeast complex, albeit with very low affinity. Taken together, our work shows that the reconstituted Mpc1/Mpc3 hetero-dimer displays the expected characteristics of the mitochondrial pyruvate carrier, providing the first direct experimental evidence of the functional unit.

Individual MPC proteins form homo-dimers but they are not functional

In the absence of other Mpc proteins, Mpc3 formed a stable homo-dimer (Fig 2C and D). The human MPC2 protein, which is related to Mpc3, was recently purified and reconstituted into liposomes and was proposed to have pyruvate transport activity (Nagampalli et al., 2018). To clarify whether the individual yeast Mpc proteins are capable of pyruvate transport, under conditions where their partner is not expressed, we purified and reconstituted Mpc1 and Mpc3 separately in liposomes and tested whether they could transport pyruvate. In parallel, the Mpc1/Mpc3 hetero-complex was used as control. While the hetero-complex mediated robust pyruvate homo-exchange at a ΔpH of 1.6, there was no measurable activity for Mpc3 or Mpc1 alone (Fig 4A and 4B). It is unlikely that this result is due to differences in reconstitution. First, the purified Mpc3 homo-dimer is as stable in detergent as the functional hetero-dimer (Fig 1D and E) and second a similar amount of Mpc3 was reconstituted into liposomes as the Mpc1/Mpc3 complex.

We were able to extend our analysis and compared the properties of the Mpc1/Mpc3 hetero-dimer with the Mpc3 homo-dimer, taking advantage of the CPM thermostability assay, where both proteins showed similar unfolding profiles (Fig 1D). It has been previously shown that binding events, creating new interactions between membrane proteins and inhibitors, result in an increased apparent melting temperature in thermostability analyses (Alexandrov et al., 2008, Crichton et al.,

2015). If inhibitors bind to MPC, their interaction with the protein should also lead to a shift in thermostability upon binding. Indeed, at saturating concentrations, Zaprinast stabilised the Mpc1/Mpc3 hetero-complex by shifting the apparent melting temperature from 53.7 to 57 °C (Fig 4C), consistent with its ability to inhibit transport. However, Zaprinast did not have an effect on the thermostability of the Mpc3 homo-dimer (Fig 4C), consistent with the inhibitor not interacting with Mpc3 alone. Unfortunately, we were not able to include UK5099 in this analysis as this coloured compound quenches the fluorescent signal, complicating interpretation. Since Mpc1 did not show an unfolding curve in the CPM analysis (Fig 1D), we tested the effect of Zaprinast on Mpc1 via nanoDSF, using Mpc1/Mpc3 as a control (Fig 4D). While the Mpc1/Mpc3 hetero-complex was stabilized by Zaprinast, no stabilizing shift was observed for Mpc1, but it is possible that the protein is not in a competent state. Overall, our results show that Mpc protomers can form homo-dimers, but they do not transport pyruvate and do not bind the inhibitor Zaprinast.

Discussion

Despite the fundamental role of MPC in metabolism and disease, little was known about its composition and mechanism of transport and inhibition. We present here robust evidence that the mitochondrial pyruvate carrier is functional as a hetero-dimer. When the Mpc protomers from *S. cerevisiae* were expressed, purified and reconstituted into liposomes in combinations, the hetero-dimeric complexes were functional, whereas the individual proteins formed inactive homo-dimers.

Our results on the yeast Mpc are different than the published results on the human MPC proteins, where a co-expression and co-purification strategy did not lead to hetero-complex formation (Nagampalli et al., 2018). Specifically, in the presence of the co-expressed MPC1, the MPC2 protein was purified alone. This is not consistent with genetic and functional analyses of mammalian MPCs, including the human MPC, where co-expression of both MPC proteins was found to be necessary for mitochondrial pyruvate carrier activity (Bricker et al., 2012, Compan et al., 2015, Herzig et al., 2012, Vanderperre et al., 2016). We show here that the co-expressed yeast Mpc proteins co-purify to form folded and stable hetero-dimers in detergent solution. It is not possible to safely conclude on the oligomeric state of the mammalian MPCs, as it could differ between species, but our strategy can be applied to characterise the mammalian MPC complexes.

Establishing the oligomeric state of MPC is a first step to understand its bioenergetics and transport mechanism. Our results directly contradict the idea that the MPC proteins form multimeric complexes of 150 kDa, as proposed previously based on blue native gel electrophoretic analysis of the yeast complex Mpc1/Mpc2 (Bricker et al., 2012). We have shown here that within a large protein-detergent-lipid complex (163.3 ± 5.7 kDa in our experimental setup), the protein contribution was only 30.8 ± 1.3 kDa, clearly corresponding to a hetero-dimer. It is likely that the anomalous migration of MPC on blue native gels is caused by binding of Coomassie stain to both the protein and the detergent-lipid micelle, as observed for other small membrane proteins (Crichton et al., 2013).

We also provide here strong evidence for the ability of the MPC hetero-dimers to transport pyruvate by measuring pyruvate homo-exchange activity, which was inhibited by previously proposed MPC inhibitors, such as UK5099, Zaprinast, lonidamine, 7ACC2 and the TZD rosiglitazone. Pyruvate exchange was dependent on the ΔpH and the measured apparent affinity for pyruvate (K_M) was in line with other studies of pyruvate transport (Gray et al., 2016, Halestrap, 1975) and pyruvate homo-exchange in isolated mitochondria (Papa & Paradies, 1974, Paradies & Papa, 1975). These results demonstrate that the hetero-dimer is the functional unit of the yeast mitochondrial pyruvate carrier. Our experimental system provides now a unique opportunity to study the detailed mechanism of pyruvate transport by the MPC hetero-complexes in yeast but also creates new opportunities for the purification and reconstitution of the human MPC hetero-complex.

Consistent with previous observations that some MPC proteins homo-oligomerise (Bender et al., 2015, Bricker et al., 2012, Nagampalli et al., 2018) we found that Mpc1 and Mpc3 can be expressed and purified individually and we showed that Mpc3 forms stable homo-dimers, but only when it is expressed individually. Under normal conditions, it engages in hetero-complex formation with Mpc1. In our system, no transport activity could be detected for Mpc1 or Mpc3 homo-dimers in conditions where the hetero-dimer showed robust transport activity. The reason might be that pyruvate is an asymmetric substrate, requiring an asymmetric binding pocket for co-ordination, which cannot be provided by a homo-dimer. Additionally, unlike the Mpc1/Mpc3 hetero-complex, the Mpc3 or Mpc1 alone did not interact with Zaprinast. Therefore, the yeast Mpc homo-dimers are not functional and they may not form a functional binding pocket.

Mpc1, Mpc2 and Mpc3 are highly homologous membrane proteins throughout the length of the conserved parts, strongly suggesting that the topology of all three must be very similar (Fig EV1). The observation that Mpc3 can form both a functional hetero-dimer with Mpc1 and non-functional homo-dimer also indicates that these proteins must have similar structures. Investigation of the secondary structure and hydropathy profile indicates that the yeast Mpc proteins may have three transmembrane α-helices each (Fig EV1). The N-terminal region also has the propensity to form an α-helix, which is amphipathic in nature, whereas the secondary structure of the C-terminal region, which is highly variable in length, is unclear. The distantly related semi-SWEET transporters, which import sugars into bacteria (Lee et al., 2015, Xu et al., 2014), have a similar topology and also dimerise.

This work provides the basis for understanding the function of the MPC hetero-complex, the detailed mechanism of substrate transport and inhibition and the substrate specificity profile. Moreover, it will pave the way towards structural analysis of the complex. These studies will be important in light of the central role of MPC in metabolism, its involvement in diseases and its potential use as a drug target.

Materials and methods

Molecular biology

The codon-optimised gene sequences for Mpc1 (UniProt: P53157), Mpc2 (UniProt: P38852) and Mpc3 (UniProt: P53311) from *S. cerevisiae* were synthesised (GenScript) and cloned into the bidirectional expression vector pBEVY-GU (gift from Charles Miller; Addgene plasmid # 51229 (Miller et al., 1998)). For expression of *mpc1*, the cDNA was subcloned into the EcoRI/SacI sites and for *mpc2* or *mpc3* into the BamHI/XbaI sites. Where indicated, the sequences were designed to include a sequence coding for Factor Xa cleavage site (IEGR), followed by an octa-histidine tag at their C-termini. For expression of individual proteins, each single sequence was subcloned in the EcoRI/SacI sites of the same vector.

Protein expression and mitochondrial preparations.

The expression plasmids were transformed into an *mpc* triple deletion strain of *S. cerevisiae* (SHY15) (Herzig et al., 2012) or into the W303-1B strain (MATα leu2-3, 112 trp1-1 can1-100 ura3-1 ade2-1 his3-11,15), using standard methods (Gietz &

Schiestl, 2007). Successful transformants were selected on synthetic-complete uracil-dropout medium (Formedium) plates supplemented with 2 % (w/v) glucose. Pre-cultures were grown in the same medium and used to inoculate 50 L of YPG medium containing 0.1 % (w/v) glucose in an Applikon Pilot Plant 140-L bioreactor (Thangaratnarajah et al., 2014). Protein expression was induced for 3 h with 0.4 % (w/v) galactose, after 20 h of growth in YPG. Mitochondrial isolation was performed, as previously described (Thangaratnarajah et al., 2014), using a DYNO-MILL (Willy A. Bachofen). Isolated mitochondria were aliquoted, flash-frozen in liquid nitrogen and stored in -80 °C until use.

Affinity chromatography

All the protomers (Mpc1, Mpc2, Mpc3) and the Mpc1/Mpc2 hetero-complex were expressed in and purified from mitochondria of the SHY15 strain. The Mpc1/Mpc3 hetero-complex was expressed in both SHY15 and W303-1B strains, and yielded the same results with respect to the Mpc1/Mpc3 protein ratio and stability. The W303-1B strain was selected for large-scale purification of Mpc1/Mpc3 based on the total protein yield. Immediately prior to purification, 1 g of mitochondria were thawed and suspended in buffer containing 20 mM Tris-HCl, pH 7.4, 150 mM NaCl, 10 % (v/v) glycerol, one Complete EDTA-free protease inhibitor cocktail tablet (Roche) and 1 % (w/v) lauryl maltose neopentyl glycol (LMNG, Anatrace). Mitochondria were solubilised for 1.5 h at 4 °C under gentle agitation, and then clarified by ultracentrifugation at 205,000 x g for 45 min. The supernatant was incubated for 2 h with nickel Sepharose beads (GE Healthcare), previously equilibrated with 20 mM Tris-HCl, pH 7.4, 150 mM NaCl, and then poured into an empty column (Bio-Rad). The column was initially washed with 20 column volumes of Buffer A (20 mM Tris-HCl, pH 7.4, 150 mM NaCl, 40 mM imidazole, 0.1 % (w/v) LMNG, 0.1 mg/ml tetraoleoyl cardiolipin (TOCL)), followed by 20 column volumes of buffer B (20 mM Tris-HCl, pH 7.4, 150 mM NaCl, 5 mM $CaCl_2$, 0.1 % (w/v) LMNG, 0.1 mg/ml TOCL). Mpc1/Mpc3 was eluted from the column by on-column digestion for 12 h at 4 °C with 10 µg of Factor Xa protease (New England Biolabs) per 1 g of mitochondria. Mpc1/Mpc2 was eluted after 1 h cleavage with Factor Xa with 10 µg of Factor Xa per 1 g of mitochondria. The mobile phase containing untagged MPC was separated from the resin with empty Proteus Midi spin columns (Generon) at 200 x g for 5 min. Protein concentration was determined by the bicinchoninic acid

assay (Thermo Fisher Scientific). Freshly purified protein was used for reconstitution into liposomes and for size-exclusion chromatography (SEC) coupled to multi-angle laser light scattering (MALLS), called SEC-MALLS.

Size-exclusion chromatography

Analytical size-exclusion chromatography was performed on an ÄKTA Explorer (GE Healthcare) with a Superdex 200 10/300 GL column (GE Healthcare) equilibrated in SEC buffer (20 mM Tris-HCl, pH 7.4, 150 mM NaCl, 0.05 % (w/v) LMNG, 0.05 mg/ml TOCL). Nickel purified proteins were injected without being concentrated onto the column at 0.3 ml/min and 0.15 ml fractions were collected. The column was calibrated with a high molecular weight calibration kit (GE Healthcare) in the same buffer without detergent and lipid.

Thermostability analysis using a thiol reactive probe

The assessment of protein stability was performed via thermal denaturation using a rotary quantitative PCR (qPCR) instrument as previously described (Crichton et al., 2015). In this method, cysteine residues, buried within the protein structure, become solvent exposed during denaturation in a temperature ramp and react with N-[4-(7-diethylamino-4-methyl-3-coumarinyl)phenyl]-maleimide (CPM) to form fluorescent-adducts. Briefly, a CPM working solution was prepared by diluting the CPM stock (5 mg/ml in dimethyl sulfoxide) 50-fold into assay solution (20 mM Tris-HCl, pH 7.4, 150 mM NaCl, 5 mM $CaCl_2$, 0.1 % (w/v) LMNG, 0.1 mg/ml TOCL), and incubated for 10 min at room temperature. For each analysis, carried out in triplicates, 3 µg of purified MPC were diluted into the same buffer to a final volume of 45 µl, to which 5 µl of the CPM working solution were added. When testing the effect of MPC inhibitors by thermostability shift assays, the protein was diluted in assay buffer containing the desired concentration of the inhibitor and then 5 µl of the CPM working solution were added. In each case, samples were incubated on ice for a further 10 min and then subjected to a temperature gradient from 25 to 90 °C at 1 °C increments with a 4 s hold, corresponding to a temperature ramp of 5.6 °C/min. The fluorescence increase was monitored with the HRM channel of the machine (excitation at 440–480 nm, emission at 505–515 nm). Unfolding profiles were analysed with the Rotor-Gene Q

software 2.3 and the peaks of their derivatives were used to determine the apparent melting temperature as a relative measure of protein stability.

Thermostability analysis by nanoDSF

The protein stability was also assessed using dye-free nano differential scanning fluorimetry (nanoDSF), which monitors fluorescence changes due to altered environments of tryptophan and tyrosine residues during unfolding. Protein samples in buffer containing 20 mM Tris-HCl pH 7.4, 150 mM NaCl, 5 mM $CaCl_2$, 0.1 % (w/v) LMNG, 0.1 mg/ml TOCL, in the presence or absence of the indicated concentrations of small molecule inhibitors, were loaded into capillary tubes, and subjected to a temperature gradient from 20 to 95 °C with a temperature ramp of 5 °C/min. The intrinsic fluorescence was measured using the NanoTemper Prometheus NT.48 instrument.

Immunoblotting

Protein concentrations of crude mitochondrial preparations, isolated from the *S. cerevisiae* SHY15 (Herzig et al., 2012) or W303-1B strains, were determined by the bicinchoninic acid assay (Pierce). Twenty-five micrograms of mitochondria were subjected to SDS-PAGE (4-20 % gradient gel) and proteins were electroblotted onto polyvinylidene difluoride (PVDF) membranes. Proteins were probed with polyclonal antibodies raised in hen against Mpc peptides (Agrisera) and detected with a rabbit anti-chicken (IgG) horseradish peroxidase conjugate (Sigma, A9046). The antibodies were raised against a synthetic peptide corresponding to residues 111-126 of Mpc1 and residues 40–54 of Mpc3. For detection of Mpc2, a mouse anti-his antibody (Roche, 04905318001) was used, followed by goat anti-mouse (IgG) horseradish peroxidase conjugate (Thermo Fisher Scientific, G21040). The signal was developed using the ECL reagent Western blot detection kit (GE Healthcare) and visualised on X-ray films.

Mass determination by SEC-MALLS

SEC-MALLS analysis was performed with a Superdex 200 10/300 GL column (GE Healthcare) on an ÄKTA Explorer (GE Healthcare) coupled in-line with a light scattering detector (Dawn HELEOSII, Wyatt Technologies) and a refractometer

(Optilab T-rREX, Wyatt Technologies). The Mpc1/Mpc3 complex or the individual Mpc3 protein were injected at 0.3 ml/min onto the Superdex 200 10/300 GL column equilibrated with 20 mM Tris-HCl, pH 7.4, 150 mM NaCl, 0.005 % (w/v) LMNG, 0.005 mg/ml TOCL. All data were recorded and analysed with ASTRA 6.03 (Wyatt Technologies). Molecular weight calculations were performed using the protein-conjugate method (Slotboom et al., 2008) with the dn/dc value for protein of 0.185 ml/g and dn/dc value for LMNG-TOCL of 0.1675 ml/g (Thangaratnarajah et al., 2014). To determine the contribution of each protein to the overall protein-detergent-lipid complex, the extinction coefficients ε_{A280} were calculated from the amino-acid sequence using the ProtParam tool on the ExPaSy server (Gasteiger et al., 2005).

Reconstitution in proteoliposomes

Egg L-α-phosphatidylcholine 99 % (Avanti Polar Lipids) and tetraoleoyl cardiolipin (Avanti Polar Lipids) were mixed in a 20:1 (w/w) ratio, dried under a stream of nitrogen and washed once with methanol before being dried again. Lipids were hydrated in 20 mM Tris-HCl, pH 8.0, 50 mM NaCl to a concentration of 12 mg/ml. Cold pyruvate to be internalised was added as a freshly made concentrated stock, where indicated. Lipids were solubilised with 1.2 % (v/v) pentaethylene glycol monodecyl ether (Sigma) and freshly purified protein was added at a lipid-to-protein ratio of 250:1 (w/w) for Mpc1/Mpc3 and 125:1 for Mpc1/Mpc2. Samples were incubated on ice for 5 min, after which liposomes were formed by the step-wise removal of pentaethylene glycol monodecyl ether by five additions of 60 mg Bio-Beads SM-2 (Bio-Rad) with gentle mixing at 4 °C at 20 min intervals. A final addition of 180 mg Bio-Beads was incubated with the samples overnight. Proteoliposomes were first separated from the Bio-Beads by passage through empty spin columns (Bio-Rad), and subsequently pelleted at 120,000 x g for 60 min. The proteoliposomes were resuspended with a thin needle in 150 µl of their supernatant after the rest of it was removed.

Pyruvate transport assays

The time course of pyruvate homo-exchange was measured at room temperature. The transport was initiated by diluting the proteoliposomes 200-fold into external

buffer, containing 50 μM [^{14}C]-pyruvate (500,000 dpm, Perkin Elmer). The external buffers of different pH were i) 20 mM MES, pH 5.4, 50 mM NaCl ii) 20 mM MES, pH 6.4, 50 mM NaCl iii) 20 mM Tris-HCl, pH 7.4, 50 mM NaCl iv) 20 mM Tris-HCl, pH 8.0, 50 mM NaCl. The reaction (0–60 s) was terminated by rapid dilution into 8 volumes of ice-cold internal buffer (20 mM Tris-HCl, pH 8.0, 50 mM NaCl or 20 mM Tris-HCl, pH 7.4, 50 mM NaCl, as indicated), followed by rapid filtration through cellulose nitrate 0.45 μm filters (Millipore) and washing with an additional 8 volumes of buffer. The filters were dissolved in Ultima Gold scintillation liquid (Perkin Elmer) and the radioactivity was counted with a Perkin Elmer Tri-Carb 2800 RT liquid scintilation counter. The initial rate measurements to determine kinetic parameters were taken after 5s of linear transport. Increasing concentrations of pyruvate were achieved by diluting the specific activity of [^{14}C]-pyruvate with unlabelled pyruvate. For inhibition of pyruvate transport various concentrations (as indicated in the Figure legends) of UK5099, Zaprinast, Ionidamine, 7ACC2, or the indicated TZDs were added to the liposomes simultaneously with 50 μM radioactive substrate. The data analysis was performed with non-linear regression fittings using GraphPad Prism 7.0d ([Inhibitor] vs response, variable slope). The specific uptake rates were calculated based on the amount of protein used in reconstitutions, as determined by bicinchoninic acid assay. The biological repeats represent independent proteoliposome preparations using fresh protein from independent purifications.

Peptide mass fingerprinting

SDS polyacrylamide gel portions were subjected to in-gel proteolytic digestion with trypsin according to standard protocols. Extracted peptide mixtures were analysed with a 4800 MALDI-TOFTOF mass spectrometer (Applied Biosystems). Peptide fragmentation spectra were matched to the NCBI non-redundant DNA sequence database version 20120611 (18480950 sequences; 6336030745 residues) using the software package Mascot version 2.4 (Matrix Science www.matrixscience.com). Peptide ion scores greater than 58 points indicate identity or extensive homology ($p<0.05$).

Data availability: Original data available on the Dryad Digital Repository. https://doi.org/10.5061/dryad.m173s71

Acknowledgments: We thank Drs. Ian Fearnley and Shujing Ding for total mass analysis performed at the MRC Mitochondrial Biology Unit and Dr. Chris Johnson for access to the NanoTemper Prometheus NT.48 at the MRC Laboratory of Molecular Biology. We also thank Dr. Shane Palmer for the large-scale fermentation and Dr. Martin S. King for providing valuable feedback on the manuscript. This work was supported by the Medical Research Council Grant MC_UU_00015/1 (to E.R.S.K.), the Swiss National Science Foundation 31003A_179421/1 (to J-C.M.) and the Oncosuisse grant KFS-4434-02-2018 (to J-C.M.).

Author contributions: S.T., C.T. and E.R.S.K. designed the research; S.T., C.T., V.M. and M.E.H. performed the research; S.T. and C.T. analysed the data; S.T., C.T, J.C.M. and E.R.S.K. wrote the paper.

Conflict of interest: The authors declare no conflict of interest.

References

Alexandrov AI, Mileni M, Chien EY, Hanson MA, Stevens RC (2008) Microscale fluorescent thermal stability assay for membrane proteins. *Structure* 16: 351-359

Bader DA, Hartig SM, Putluri V, Foley C, Hamilton MP, Smith EA, Saha PK, Panigrahi A, Walker C, Zong L, Martini-Stoica H, Chen R, Rajapakshe K, Coarfa C, Sreekumar A, Mitsiades N, Bankson JA, Ittmann MM, O'Malley BW, Putluri N et al. (2019) Mitochondrial pyruvate import is a metabolic vulnerability in androgen receptor-driven prostate cancer. *Nature Metabolism* 1: 70-85

Bakker EP, van Dam K (1974) The movement of monocarboxylic acids across phospholipid membranes: evidence for an exchange diffusion between pyruvate and other monocarboxylate ions. *Biochimica et biophysica acta* 339: 285-289

Bender T, Pena G, Martinou JC (2015) Regulation of mitochondrial pyruvate uptake by alternative pyruvate carrier complexes. *The EMBO journal* 34: 911-924

Bricker DK, Taylor EB, Schell JC, Orsak T, Boutron A, Chen YC, Cox JE, Cardon CM, Van Vranken JG, Dephoure N, Redin C, Boudina S, Gygi SP, Brivet M, Thummel CS, Rutter J (2012) A mitochondrial pyruvate carrier required for pyruvate uptake in yeast, Drosophila, and humans. *Science* 337: 96-100

Buchan DW, Minneci F, Nugent TC, Bryson K, Jones DT (2013) Scalable web services for the PSIPRED Protein Analysis Workbench. *Nucleic acids research* 41: W349-357

Chen Y, McCommis KS, Ferguson D, Hall AM, Harris CA, Finck BN (2018) Inhibition of the Mitochondrial Pyruvate Carrier by Tolylfluanid. *Endocrinology* 159: 609-621

Colca JR, McDonald WG, Cavey GS, Cole SL, Holewa DD, Brightwell-Conrad AS, Wolfe CL, Wheeler JS, Coulter KR, Kilkuskie PM, Gracheva E, Korshunova Y, Trusgnich M, Karr R, Wiley SE, Divakaruni AS, Murphy AN, Vigueira PA, Finck BN, Kletzien RF (2013) Identification of a mitochondrial target of thiazolidinedione insulin sensitizers (mTOT)--relationship to newly identified mitochondrial pyruvate carrier proteins. *PloS one* 8: e61551

Colca JR, Tanis SP, McDonald WG, Kletzien RF (2014) Insulin sensitizers in 2013: new insights for the development of novel therapeutic agents to treat metabolic diseases. *Expert Opin Investig Drugs* 23: 1-7

Compan V, Pierredon S, Vanderperre B, Krznar P, Marchiq I, Zamboni N, Pouyssegur J, Martinou JC (2015) Monitoring Mitochondrial Pyruvate Carrier Activity in Real Time Using a BRET-Based Biosensor: Investigation of the Warburg Effect. *Molecular cell* 59: 491-501

Corbet C, Bastien E, Draoui N, Doix B, Mignion L, Jordan BF, Marchand A, Vanherck JC, Chaltin P, Schakman O, Becker HM, Riant O, Feron O (2018) Interruption of lactate uptake by inhibiting mitochondrial pyruvate transport unravels direct antitumor and radiosensitizing effects. *Nature communications* 9: 1208

Crichton PG, Harding M, Ruprecht JJ, Lee Y, Kunji ER (2013) Lipid, detergent, and Coomassie Blue G-250 affect the migration of small membrane proteins in blue native gels: mitochondrial carriers migrate as monomers not dimers. *The Journal of biological chemistry* 288: 22163-22173

Crichton PG, Lee Y, Ruprecht JJ, Cerson E, Thangaratnarajah C, King MS, Kunji ER (2015) Trends in thermostability provide information on the nature of substrate, inhibitor, and lipid interactions with mitochondrial carriers. *The Journal of biological chemistry* 290: 8206-8217

Divakaruni AS, Wallace M, Buren C, Martyniuk K, Andreyev AY, Li E, Fields JA, Cordes T, Reynolds IJ, Bloodgood BL, Raymond LA, Metallo CM, Murphy AN (2017) Inhibition of the mitochondrial pyruvate carrier protects from excitotoxic neuronal death. *J Cell Biol* 216: 1091-1105

Divakaruni AS, Wiley SE, Rogers GW, Andreyev AY, Petrosyan S, Loviscach M, Wall EA, Yadava N, Heuck AP, Ferrick DA, Henry RR, McDonald WG, Colca JR, Simon MI, Ciaraldi TP, Murphy AN (2013) Thiazolidinediones are acute, specific inhibitors of the mitochondrial pyruvate carrier. *Proceedings of the National Academy of Sciences of the United States of America* 110: 5422-5427

Du J, Cleghorn WM, Contreras L, Lindsay K, Rountree AM, Chertov AO, Turner SJ, Sahaboglu A, Linton J, Sadilek M, Satrustegui J, Sweet IR, Paquet-Durand F, Hurley JB (2013) Inhibition of mitochondrial pyruvate transport by zaprinast causes massive accumulation of aspartate at the expense of glutamate in the retina. *The Journal of biological chemistry* 288: 36129-36140

Gasteiger E, Hoogland C, Gattiker A, Duvaud Se, Wilkins MR, Appel RD, Bairoch A (2005) Protein Identification and Analysis Tools on the ExPASy Server. In *The Proteomics Protocols Handbook*, Walker JM (ed) pp 571-607. Humana Press

Ghosh A, Tyson T, George S, Hildebrandt EN, Steiner JA, Madaj Z, Schulz E, Machiela E, McDonald WG, Escobar Galvis ML, Kordower JH, Van Raamsdonk JM, Colca JR, Brundin P (2016) Mitochondrial pyruvate carrier regulates autophagy, inflammation, and neurodegeneration in experimental models of Parkinson's disease. *Sci Transl Med* 8: 368ra174

Gietz RD, Schiestl RH (2007) High-efficiency yeast transformation using the LiAc/SS carrier DNA/PEG method. *Nat Protoc* 2: 31-34

Gray LR, Rauckhorst AJ, Taylor EB (2016) A Method for Multiplexed Measurement of Mitochondrial Pyruvate Carrier Activity. *The Journal of biological chemistry* 291: 7409-7417

Gray LR, Sultana MR, Rauckhorst AJ, Oonthonpan L, Tompkins SC, Sharma A, Fu X, Miao R, Pewa AD, Brown KS, Lane EE, Dohlman A, Zepeda-Orozco D, Xie J, Rutter J, Norris AW, Cox JE, Burgess SC, Potthoff MJ, Taylor EB (2015) Hepatic Mitochondrial Pyruvate Carrier 1 Is Required for Efficient Regulation of Gluconeogenesis and Whole-Body Glucose Homeostasis. *Cell Metab* 22: 669-681

Halestrap AP (1975) The mitochondrial pyruvate carrier. Kinetics and specificity for substrates and inhibitors. *The Biochemical journal* 148: 85-96

Halestrap AP (1976) The mechanism of the inhibition of the mitochondrial pyruvate transportater by alpha-cyanocinnamate derivatives. *The Biochemical journal* 156: 181-183

Halestrap AP (2012) The mitochondrial pyruvate carrier: has it been unearthed at last? *Cell Metab* 16: 141-143

Halestrap AP, Denton RM (1974) Specific inhibition of pyruvate transport in rat liver mitochondria and human erythrocytes by alpha-cyano-4-hydroxycinnamate. *The Biochemical journal* 138: 313-316

Herzig S, Raemy E, Montessuit S, Veuthey JL, Zamboni N, Westermann B, Kunji ER, Martinou JC (2012) Identification and functional expression of the mitochondrial pyruvate carrier. *Science* 337: 93-96

Jones DT, Taylor WR, Thornton JM (1994) A model recognition approach to the prediction of all-helical membrane protein structure and topology. *Biochemistry* 33: 3038-3049

Klingenberg M (1970) Mitochondria metabolite transport. *FEBS letters* 6: 145-154

Lee Y, Nishizawa T, Yamashita K, Ishitani R, Nureki O (2015) Structural basis for the facilitative diffusion mechanism by SemiSWEET transporter. *Nat Commun* 6: 6112

Li X, Han G, Li X, Kan Q, Fan Z, Li Y, Ji Y, Zhao J, Zhang M, Grigalavicius M, Berge V, Goscinski MA, Nesland JM, Suo Z (2017) Mitochondrial pyruvate carrier function determines cell stemness and metabolic reprogramming in cancer cells. *Oncotarget* 8: 46363-46380

Li X, Ji Y, Han G, Li X, Fan Z, Li Y, Zhong Y, Cao J, Zhao J, Zhang M, Wen J, Goscinski MA, Nesland JM, Suo Z (2016) MPC1 and MPC2 expressions are associated with favorable clinical outcomes in prostate cancer. *BMC Cancer* 16: 894

McCommis KS, Chen Z, Fu X, McDonald WG, Colca JR, Kletzien RF, Burgess SC, Finck BN (2015) Loss of Mitochondrial Pyruvate Carrier 2 in the Liver Leads to Defects in Gluconeogenesis and Compensation via Pyruvate-Alanine Cycling. *Cell Metab* 22: 682-694

McCommis KS, Hodges WT, Bricker DK, Wisidagama DR, Compan V, Remedi MS, Thummel CS, Finck BN (2016) An ancestral role for the mitochondrial pyruvate carrier in glucose-stimulated insulin secretion. *Mol Metab* 5: 602-614

Miller CA, 3rd, Martinat MA, Hyman LE (1998) Assessment of aryl hydrocarbon receptor complex interactions using pBEVY plasmids: expressionvectors with bi-directional promoters for use in Saccharomyces cerevisiae. *Nucleic Acids Res* 26: 3577-3583

Nagampalli RSK, Quesnay JEN, Adamoski D, Islam Z, Birch J, Sebinelli HG, Girard R, Ascencao CFR, Fala AM, Pauletti BA, Consonni SR, de Oliveira JF, Silva ACT, Franchini KG, Leme AFP, Silber AM, Ciancaglini P, Moraes I, Dias SMG, Ambrosio ALB (2018) Human mitochondrial pyruvate carrier 2 as an autonomous membrane transporter. *Sci Rep* 8: 3510

Nancolas B, Guo L, Zhou R, Nath K, Nelson DS, Leeper DB, Blair IA, Glickson JD, Halestrap AP (2016) The anti-tumour agent lonidamine is a potent inhibitor of the mitochondrial pyruvate carrier and plasma membrane monocarboxylate transporters. *The Biochemical journal* 473: 929-936

Nanjan MJ, Mohammed M, Prashantha Kumar BR, Chandrasekar MJN (2018) Thiazolidinediones as antidiabetic agents: A critical review. *Bioorg Chem* 77: 548-567

Nath K, Guo L, Nancolas B, Nelson DS, Shestov AA, Lee SC, Roman J, Zhou R, Leeper DB, Halestrap AP, Blair IA, Glickson JD (2016) Mechanism of antineoplastic activity of lonidamine. *Biochimica et biophysica acta* 1866: 151-162

Ohashi T, Eguchi H, Kawamoto K, Konno M, Asai A, Colvin H, Ueda Y, Takaoka H, Iwagami Y, Yamada D, Asaoka T, Noda T, Wada H, Gotoh K, Kobayashi S, Koseki J,

Satoh T, Ogawa K, Doki Y, Mori M et al. (2018) Mitochondrial pyruvate carrier modulates the epithelial-mesenchymal transition in cholangiocarcinoma. *Oncol Rep* 39: 1276-1282

Papa S, Francavilla A, Paradies G, Meduri B (1971) The transport of pyruvate in rat liver mitochondria. *FEBS letters* 12: 285-288

Papa S, Paradies G (1974) On the mechanism of translocation of pyruvate and other monocarboxylic acids in rat-liver mitochondria. *European journal of biochemistry / FEBS* 49: 265-274

Paradies G, Papa S (1975) The transport of monocarboxylic oxoacids in rat liver mitochondria. *FEBS letters* 52: 149-152

Quansah E, Peelaerts W, Langston JW, Simon DK, Colca J, Brundin P (2018) Targeting energy metabolism via the mitochondrial pyruvate carrier as a novel approach to attenuate neurodegeneration. *Mol Neurodegener* 13: 28

Schell JC, Olson KA, Jiang L, Hawkins AJ, Van Vranken JG, Xie J, Egnatchik RA, Earl EG, DeBerardinis RJ, Rutter J (2014) A role for the mitochondrial pyruvate carrier as a repressor of the Warburg effect and colon cancer cell growth. *Molecular cell* 56: 400-413

Schell JC, Wisidagama DR, Bensard C, Zhao H, Wei P, Tanner J, Flores A, Mohlman J, Sorensen LK, Earl CS, Olson KA, Miao R, Waller TC, Delker D, Kanth P, Jiang L, DeBerardinis RJ, Bronner MP, Li DY, Cox JE et al. (2017) Control of intestinal stem cell function and proliferation by mitochondrial pyruvate metabolism. *Nat Cell Biol* 19: 1027-1036

Sievers F, Wilm A, Dineen D, Gibson TJ, Karplus K, Li W, Lopez R, McWilliam H, Remmert M, Soding J, Thompson JD, Higgins DG (2011) Fast, scalable generation of high-quality protein multiple sequence alignments using Clustal Omega. *Mol Syst Biol* 7: 539

Slotboom DJ, Duurkens RH, Olieman K, Erkens GB (2008) Static light scattering to characterize membrane proteins in detergent solution. *Methods* 46: 73-82

Soccio RE, Chen ER, Lazar MA (2014) Thiazolidinediones and the promise of insulin sensitization in type 2 diabetes. *Cell Metab* 20: 573-591

ter Beek J, Duurkens RH, Erkens GB, Slotboom DJ (2011) Quaternary structure and functional unit of energy coupling factor (ECF)-type transporters. *The Journal of biological chemistry* 286: 5471-5475

Thangaratnarajah C, Ruprecht JJ, Kunji ERS (2014) Calcium-induced conformational changes of the regulatory domain of human mitochondrial aspartate/glutamate carriers. *Nat Commun* 5: 5491

Vadvalkar SS, Matsuzaki S, Eyster CA, Giorgione JR, Bockus LB, Kinter CS, Kinter M, Humphries KM (2017) Decreased Mitochondrial Pyruvate Transport Activity in the Diabetic Heart: ROLE OF MITOCHONDRIAL PYRUVATE CARRIER 2 (MPC2) ACETYLATION. *The Journal of biological chemistry* 292: 4423-4433

Vanderperre B, Bender T, Kunji ER, Martinou JC (2015) Mitochondrial pyruvate import and its effects on homeostasis. *Curr Opin Cell Biol* 33: 35-41

Vanderperre B, Cermakova K, Escoffier J, Kaba M, Bender T, Nef S, Martinou JC (2016) MPC1-like Is a Placental Mammal-specific Mitochondrial Pyruvate Carrier Subunit Expressed in Postmeiotic Male Germ Cells. *The Journal of biological chemistry* 291: 16448-16461

Vigueira PA, McCommis KS, Schweitzer GG, Remedi MS, Chambers KT, Fu X, McDonald WG, Cole SL, Colca JR, Kletzien RF, Burgess SC, Finck BN (2014) Mitochondrial pyruvate carrier 2 hypomorphism in mice leads to defects in glucose-stimulated insulin secretion. *Cell reports* 7: 2042-2053

Wen J, Arakawa T, Philo JS (1996) Size-exclusion chromatography with on-line light-scattering, absorbance, and refractive index detectors for studying proteins and their interactions. *Anal Biochem* 240: 155-166

Xu Y, Tao Y, Cheung LS, Fan C, Chen LQ, Xu S, Perry K, Frommer WB, Feng L (2014) Structures of bacterial homologues of SWEET transporters in two distinct conformations. *Nature* 515: 448-452

Yang C, Ko B, Hensley CT, Jiang L, Wasti AT, Kim J, Sudderth J, Calvaruso MA, Lumata L, Mitsche M, Rutter J, Merritt ME, DeBerardinis RJ (2014) Glutamine oxidation maintains the TCA cycle and cell survival during impaired mitochondrial pyruvate transport. *Molecular cell* 56: 414-424

Zahlten RN, Hochberg AA, Stratman FW, Lardy HA (1972) Pyruvate uptake in rat liver mitochondria: Transport or adsorption? *FEBS letters* 21: 11-13

Zhong Y, Li X, Yu D, Li X, Li Y, Long Y, Yuan Y, Ji Z, Zhang M, Wen JG, Nesland JM, Suo Z (2015) Application of mitochondrial pyruvate carrier blocker UK5099 creates metabolic reprogram and greater stem-like properties in LnCap prostate cancer cells in vitro. *Oncotarget* 6: 37758-37769

Figure Legends

Figure 1 - Purification and stability analysis of Mpc proteins.

A Strategy for purification of the Mpc1/Mpc3 hetero-complex by nickel-affinity chromatography.

B Expression of Mpc proteins in mitochondria assessed by SDS-PAGE and immunoblot analysis of crude mitochondrial preparations. The individual untagged Mpc1 (Mpc1), histidine-tagged Mpc1 (Mpc1his), histidine-tagged Mpc3 (Mpc3his) or the Mpc1/Mpc3 hetero-complex (Mpc1/Mpc3his) were detected with antibodies raised against Mpc1 (left panel) or Mpc3 (right panel) and are shown with dashed arrows.

C Five micrograms of each affinity-purified Mpc protein were analysed by SDS-PAGE and the bands were visualised by Coomassie Blue stain. Peptide mass finger printing was used to identify the major protein bands (Table EV1).

D The stability of the purified proteins was assessed via thermal denaturation by fluorescent CPM-adduct formation. The thermal denaturation profiles (*left*) were used to calculate the first derivative (*right*), which provides the apparent melting temperature, indicated with the same colour coding.

E The stability of the same samples, as in panel (D), was assessed by NanoDSF. The changes in the 330 nm/350 nm ratio with temperature (*left*) were used to calculate the first derivative (*right*). Color coding is as in panel (D).

Figure 2 - The Mpc proteins form dimeric complexes.

A Nickel-affinity-purified Mpc1/Mpc3 hetero-complex used for SEC-MALLS analysis, showing a 1:1 stoichiometry of the protomers.

B SEC-MALLS analysis of the hetero-complex. The light scattering trace for Mpc1/Mpc3 is shown as a black line. The masses of the protein-detergent-lipid complex (PDL, green), the detergent-lipid micelle (DL, blue) and the protein (P, red) are indicated. Protein fractions across the peak were assessed by SDS-PAGE and visualised by Coomassie Blue staining (B, inset).

C Nickel-affinity-purified Mpc3 protein used for SEC-MALLS analysis.

D SEC-MALLS analysis of Mpc3, colour designation as in (B). The protein fractions across the peak (D, inset) were assessed as in (B).

Data information: Data in (B and D) represent a characteristic experiment repeated independently five times for Mpc1/Mpc3 and three times for Mpc3. All biological repeats are summarised in Table EV2.

Figure 3 - The Mpc1/Mpc3 hetero-complex transports pyruvate.

A Time course of pyruvate homo-exchange by the Mpc1/Mpc3 hetero-complex in liposomes (n=8) in comparison to empty liposomes (n=6) at a ΔpH of 1.6.

B Kinetic analysis of pyruvate homo-exchange at ΔpH of 1.6 (n=3). The hetero-complex was assayed for initial rates of uptake in the concentration range of 25-600 μM. The calculated K_M was 299 μM in this experiment and 318 and 409 μM in two additional biological repeats.

C Time course of pyruvate homo-exchange by the Mpc1/Mpc3 hetero-complex in physiological pH (n=4) compared to empty liposomes (n=4).

D In the absence of a ΔpH, the time course of pyruvate homo-exchange was similar for the Mpc1/Mpc3 proteoliposomes and the empty liposomes (n=4).

E Inhibition of [^{14}C]-pyruvate homo-exchange by UK5099 (1–100 μM), Zaprinast (1–1000 μM), Ionidamine (10–10000 μM) and 7ACC2 (5–500 μM). Data points represent the mean of three technical replicates of a typical experiment. The IC_{50} measurements have also been independently replicated, three times for UK5099 Zaprinast and 7ACC2 (average IC_{50} 9 ± 7 μM, 18 ± 8 μM and 27 ± 13 μM, respectively) and two times for Ionidamine (average IC_{50}, 118 ± 24 μM).

F [^{14}C]-pyruvate homo-exchange inhibition by the TZDs, pioglitazone and rosiglitazone (n=6).

Data information: Data have been independently replicated: (A) four biological repeats, (B) three biological repeats, (C, D) 2 biological repeats (E, F) three biological repeats for UK5099, Zaprinast, 7ACC2 and two biological repeats for lonidamine and the TZDs. The error bars represent the standard error of the mean in (A) and the standard deviation in (C, D and F).

Figure 4 - Mpc1 or Mpc3 alone are not functional.

A Time course of pyruvate homo-exchange in proteoliposomes at a ΔpH of 1.6 was compared for Mpc3 (n=4), the Mpc1/Mpc3 hetero-complex (n=6) and empty liposomes (n=4).

B Time course of pyruvate homo-exchange at a ΔpH of 1.6 was compared for Mpc1 (n=4), Mpc1/Mpc3 hetero-complex (n=4) and empty liposomes (n=4).

C Thermostability analysis via cpm. In detergent solution, Zaprinast (250 µM) increased the thermostability of the Mpc1/Mpc3 hetero-complex (black lines) (n=3) but not of Mpc3 (blue lines) (n=3).

D Thermostability analysis via nanoDSF. In detergent solution, Zaprinast (250 µM) increased the thermostability of the Mpc1/Mpc3 hetero-complex (black lines) (n=3) but not of Mpc1 (orange lines) (n=3).

Data information: Data have been independently replicated in two biological repeats. The error bars represent standard deviations.

Expanded View Figure Legends

Figure EV1 - Topology of yeast Mpc1, Mpc2 and Mpc3.

The alignment was generated by Clustal Omega and by manual curation (Sievers et al., 2011). The aligned residues are coloured by the ZAPPO colour scheme in which aliphatic, polar, aromatic, positively charged, negatively charged, Pro/Gly and Cys, are coloured pink, green, orange, blue, red, magenta and yellow, respectively. The asterisks indicate identical residues and the colon conserved substitutions. Also indicated are putative transmembrane helices, loop regions and the N-terminal amphipathic helix. The secondary structure elements were assigned based on PSIPRED (Buchan et al., 2013), MEMSAT3 (Jones et al., 1994) and conservation analysis.

Figure EV2 - The Mpc1/Mpc3 hetero-complex purified in different detergents.

The Mpc1/Mpc13p hetero-complex was purified in *n*-dodecyl β-D-maltoside (DDM), decyl maltose neopentyl glycol (DMNG) or Triton X-100. The solubilisation of mitochondria was performed as under Materials and Methods but in buffer containing 2 % (w/v) DDM or DMNG or 1% Triton X-100. For affinity purification, the Nickel Sepharose columns were washed with wash buffers containing 0.1 % (w/v) DDM, DMNG or Triton X-100 supplemented with 0.1 mg/ml tetraoleoyl cardiolipin (TOCL). The samples are the solubilisate of mitochondria (Sol), proteins remaining on the resin after Factor Xa cleavage (B) and flow-through from the resin (FT). Asterisks indicate the Mpc1 and Mpc3 proteins.

Figure EV3 - Size-exclusion chromatography.

A Size-exclusion chromatography of 500 µg nickel-affinity purified Mpc1/Mpc3 hetero-complex. In the A_{280} profiles, the Mpc1/Mpc3 hetero-complex was present in a symmetrical peak.

B Size-exclusion chromatography of 150 µg nickel-affinity purified Mpc3. Mpc3 produced a peak similar to that of Mpc1/Mpc3.

Data information: Insets in (**A** and **B) show** peak fractions collected and analysed by SDS-PAGE and visualised by Coomassie Blue stain.

Figure EV4 - Purification and stability analysis of the hetero-complex Mpc1/Mpc2.

A The individual histidine-tagged Mpc1 (Mpc1his), histidine-tagged Mpc2 (Mpc2his) or the Mpc1/Mpc2 hetero-complex (Mpc1/Mpc2his) were expressed in the triple *mpc* knock-out strain SHY15 and detected with antibodies raised against Mpc1 (left) or against the histidine tag (right).

B SDS-PAGE analysis of purified Mpc1, Mpc2 and Mpc1/Mpc2 proteins, visualised with Coomassie Blue stain. As the yield of the purified Mpc2 was very low, the protein was not visible with Coomassie Blue stain, but was identified on the gel by peptide mass finger printing (Table EV1).

C The stability of the purified Mpc1/Mpc2 or Mpc2 was assessed via the CPM method. Thermal denaturation profiles (*upper panel*) were used to calculate the first derivative of the data (*lower panel*). The number is the apparent melting temperature for the Mpc1/Mpc2 hetero-complex.

D Time course of pyruvate homo-exchange by the Mpc1/Mpc2 hetero-complex in liposomes in comparison to empty liposomes at a ΔpH of 1.6 (n=2).

Figure EV5 – Effect of pH on pyruvate homo-exchange in Mpc1/Mpc3-containing proteoliposomes compared to diffusion of pyruvate into empty liposomes.

Pyruvate homo-exchange of Mpc1/Mpc3 proteoliposomes or empty liposomes was tested in three conditions.

A In the absence of a ΔpH, using an internal buffer pH of 7.4 and external buffer pH of 7.4 (n=2).

B At a ΔpH of 1.0, using an internal buffer pH of 7.4 and external buffer pH of 6.4 (n=4).

C At a ΔpH of 2.0, using an internal buffer pH of 7.4 and external buffer pH of 5.4 (n=2).

Table 1 - Stoichiometry analysis of the Mpc1/Mpc3 complex.

Mpc1	Mpc3	Absorbance 0.1 % (= 1 g L^{-1})	*In silico* calculated M_w (kDa)	M_w from SEC-MALLS (kDa)	Difference (kDa)
Monomer					
1	0	1.628	15	32.92	17.92
0	1	1.868	17.12	28.69	11.57
Homo-dimer					
2	0	1.633	29.97	32.9	2.93
0	2	1.869	34.21	28.68	-5.53
Hetero-dimer					
1	1	1.757	32.1	30.83	-1.27
Homo-trimer					
3	0	1.629	44.95	32.9	-12.05
0	3	1.869	51.31	29.6	-21.71
Hetero-trimer					
2	1	1.716	47.07	31.21	-15.86
1	2	1.796	49.19	30.12	-19.07

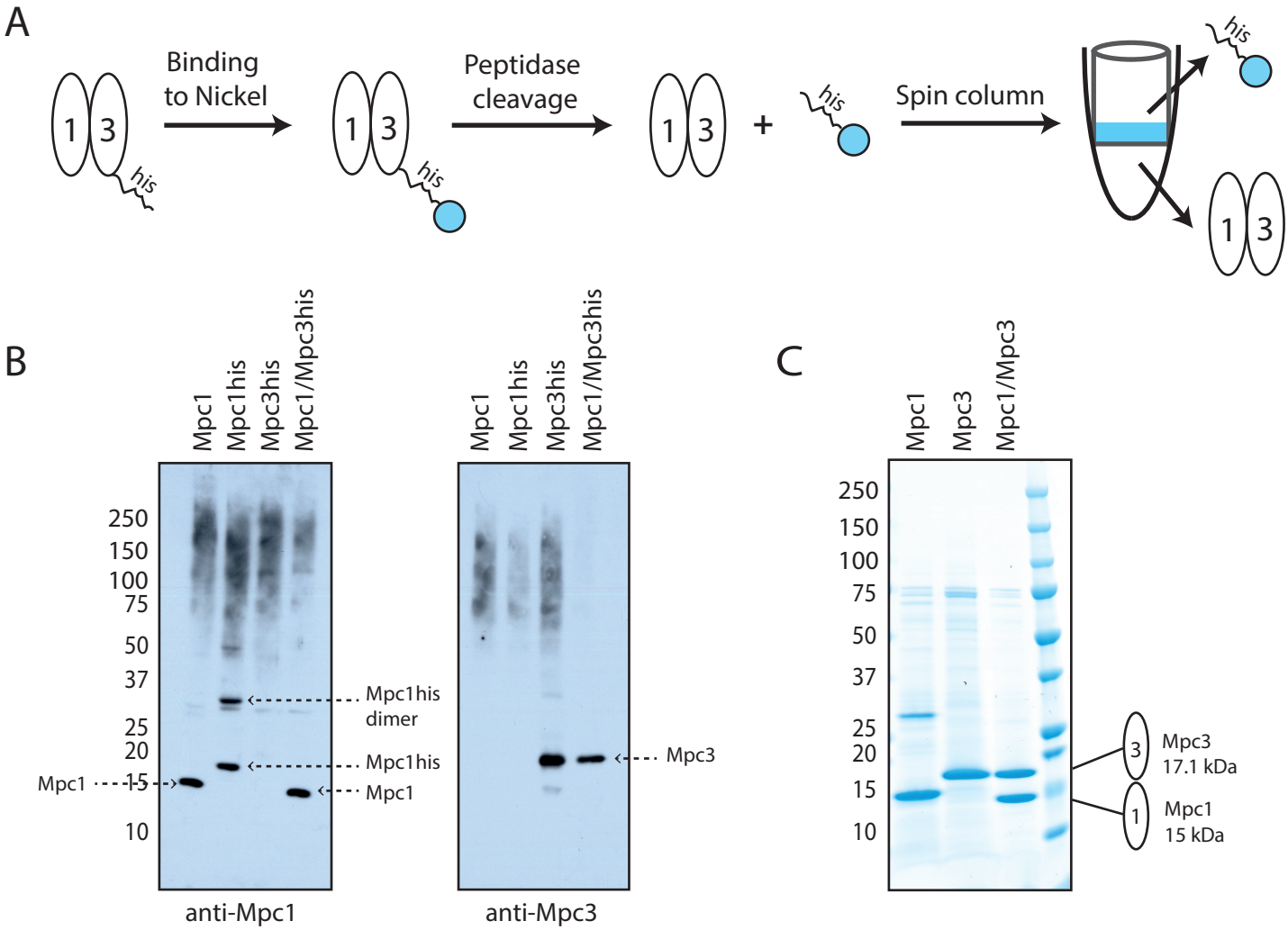
A
Binding
to Nickel
Peptidase
cleavage
Spin column
his
B
Mpc1
Mpc1his
Mpc3his
Mpc1/Mpc3his
250
150
100
75
50
37
25
20
15
10
Mpc1his
dimer
Mpc1his
Mpc1
Mpc1
Mpc3
anti-Mpc1
anti-Mpc3
C
Mpc1
Mpc3
Mpc1/Mpc3
Mpc3
17.1 kDa
Mpc1
15 kDa

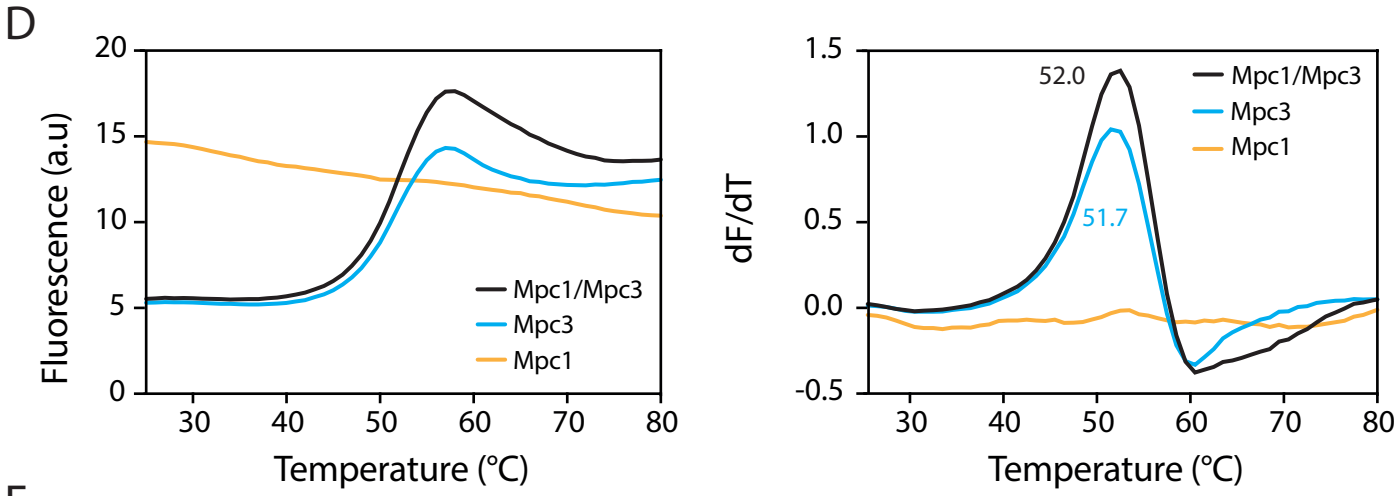
D
Fluorescence (a.u)
Temperature (°C)
Mpc1/Mpc3
Mpc3
Mpc1
dF/dT
52.0
51.7

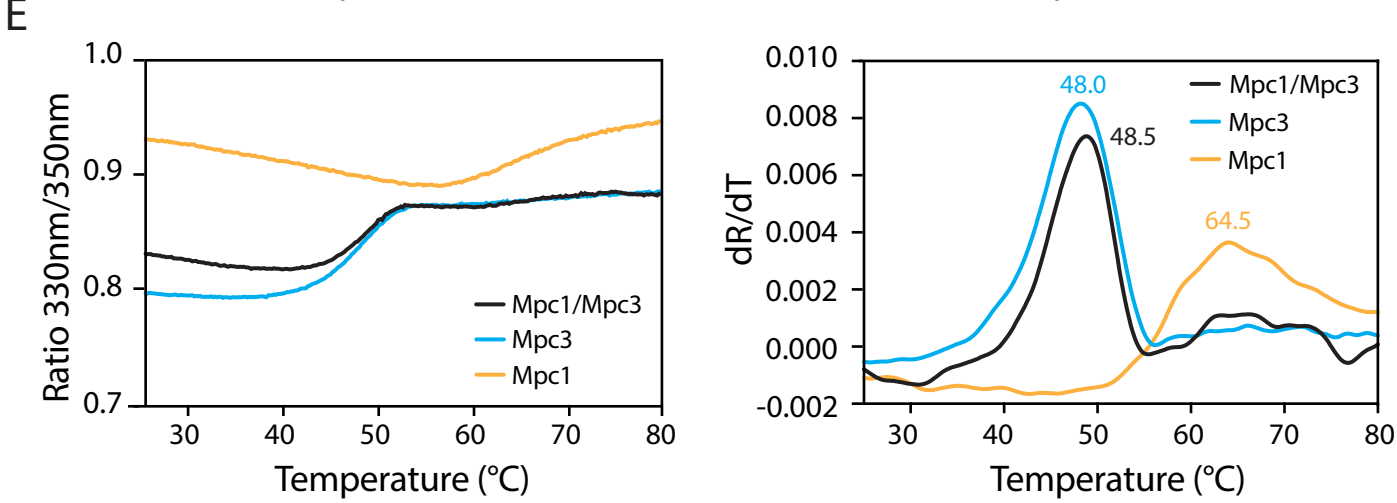
E
Ratio 330nm/350nm
Temperature (°C)
Mpc1/Mpc3
Mpc3
Mpc1
dR/dT
48.0
48.5
64.5

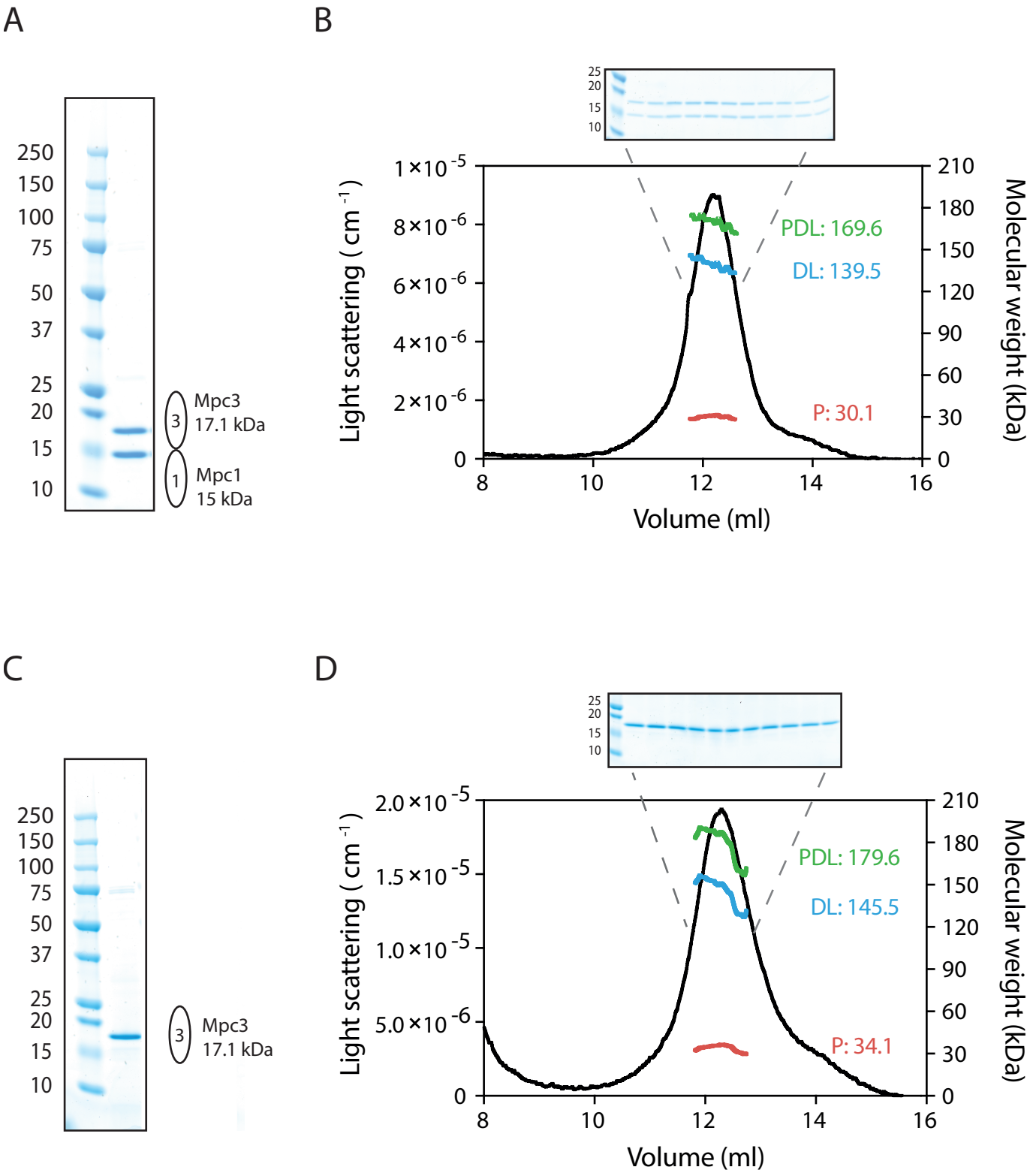
A
250
150
100
75
50
37
25
20
15
10
3
Mpc3
17.1 kDa
1
Mpc1
15 kDa
B
25
20
15
10
1×10-5
8×10-6
6×10-6
4×10-6
2×10-6
0
Light scattering (cm -1)
PDL: 169.6
DL: 139.5
P: 30.1
210
180
150
120
90
60
30
0
Molecular weight (kDa)
8
10
12
14
16
Volume (ml)
C
250
150
100
75
50
37
25
20
15
10
3
Mpc3
17.1 kDa
D
25
20
15
10
2.0×10-5
1.5×10-5
1.0×10-5
5.0×10-6
0
Light scattering (cm -1)
PDL: 179.6
DL: 145.5
P: 34.1
210
180
150
120
90
60
30
0
Molecular weight (kDa)
8
10
12
14
16
Volume (ml)

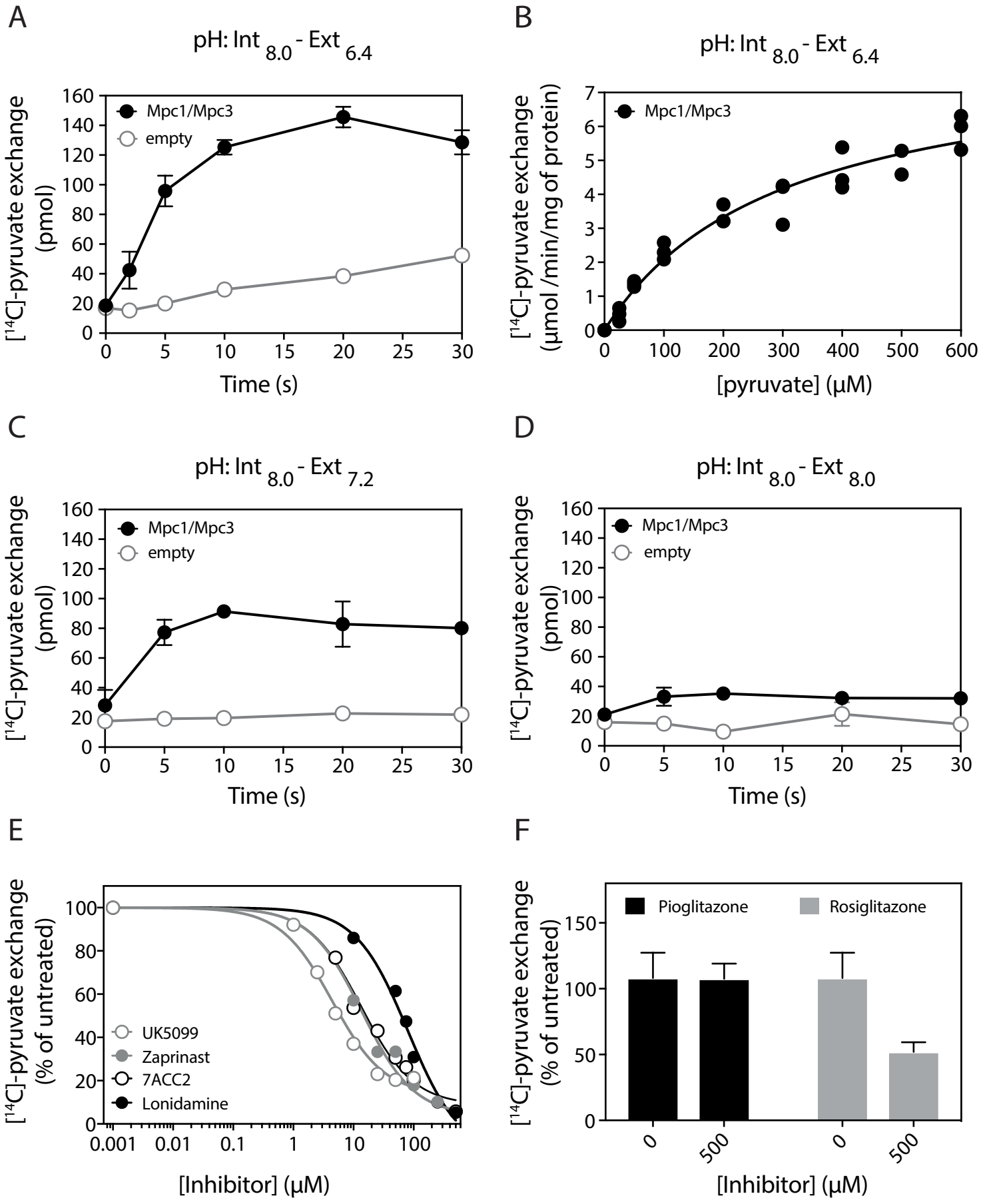
A
pH: Int 8.0 - Ext 6.4
[14C]-pyruvate exchange (pmol)
Mpc1/Mpc3
empty
Time (s)
B
pH: Int 8.0 - Ext 6.4
[14C]-pyruvate exchange (µmol /min/mg of protein)
Mpc1/Mpc3
[pyruvate] (µM)
C
pH: Int 8.0 - Ext 7.2
[14C]-pyruvate exchange (pmol)
Mpc1/Mpc3
empty
Time (s)
D
pH: Int 8.0 - Ext 8.0
[14C]-pyruvate exchange (pmol)
Mpc1/Mpc3
empty
Time (s)
E
[14C]-pyruvate exchange (% of untreated)
UK5099
Zaprinast
7ACC2
Lonidamine
[Inhibitor] (µM)
F
[14C]-pyruvate exchange (% of untreated)
Pioglitazone
Rosiglitazone
[Inhibitor] (µM)

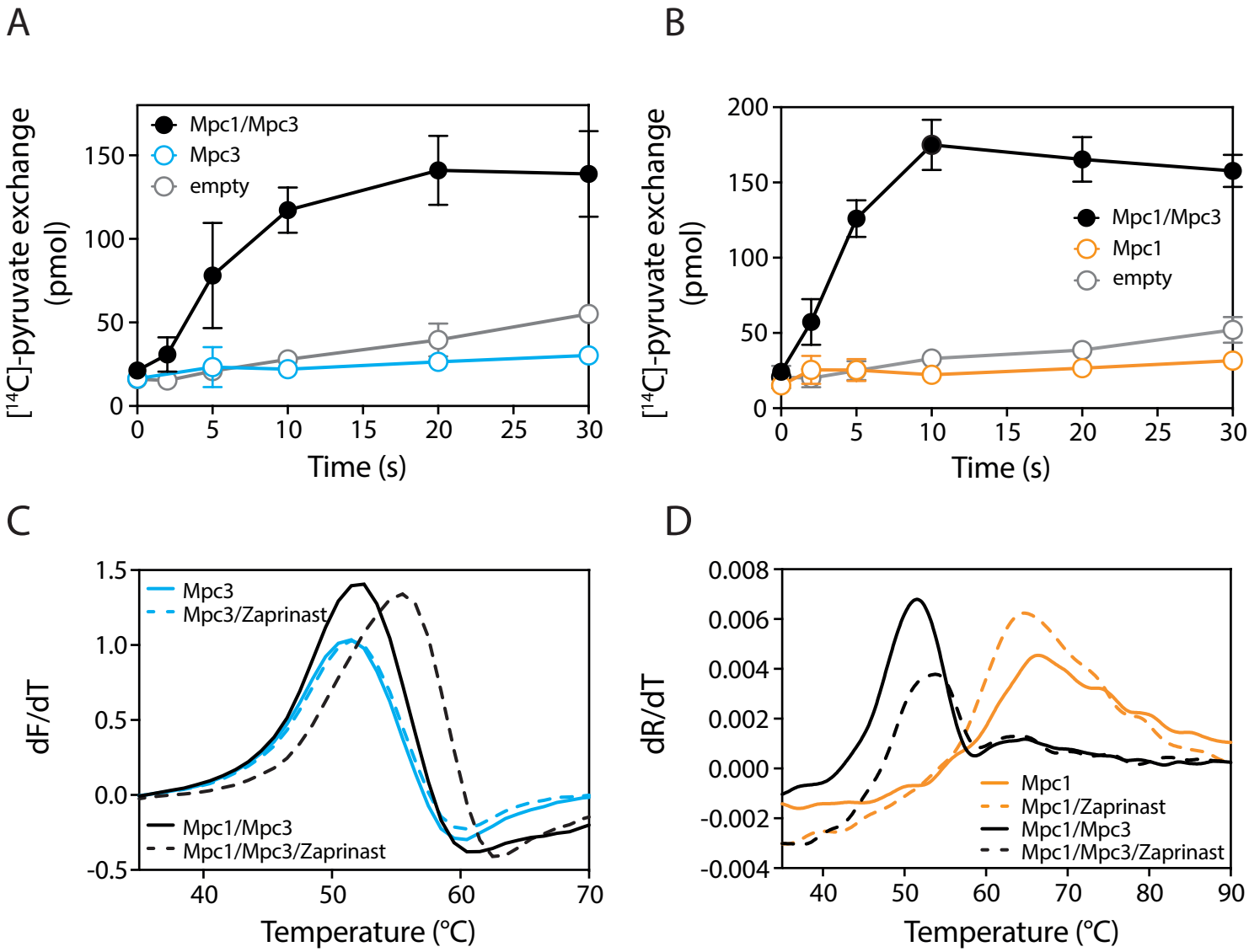
A
B
C
D
[14C]-pyruvate exchange (pmol)
Time (s)
Mpc1/Mpc3
Mpc3
empty
Mpc1
dF/dT
dR/dT
Temperature (°C)
Mpc3/Zaprinast
Mpc1/Mpc3/Zaprinast
Mpc1/Zaprinast

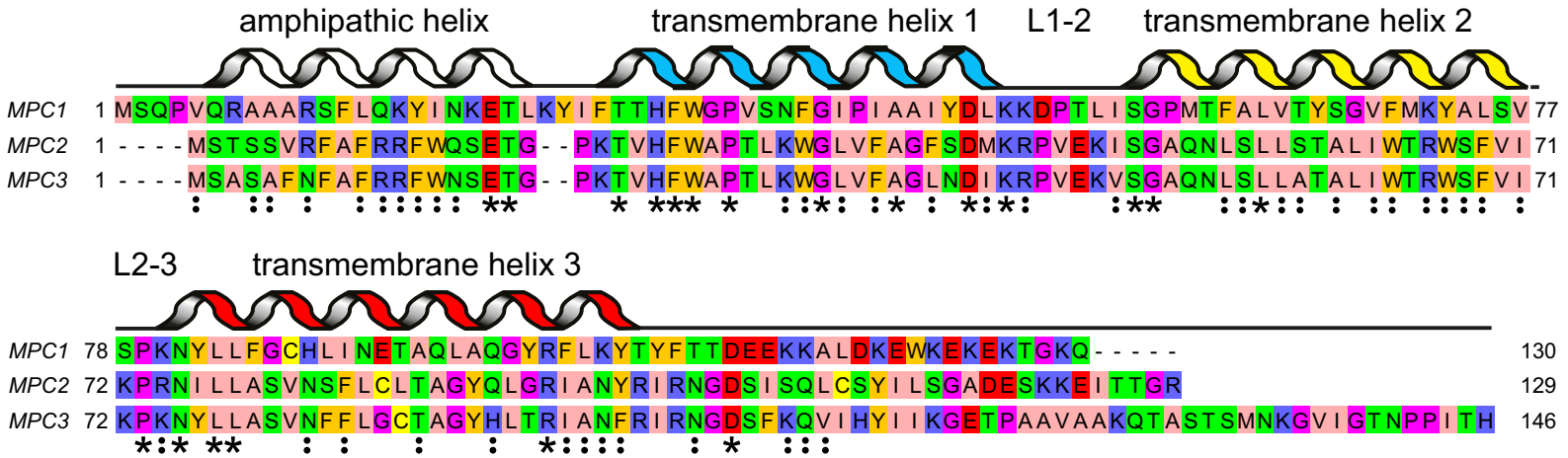
amphipathic helix
transmembrane helix 1
L1-2
transmembrane helix 2
MPC1 1 MSQPVQRAAARSFLQKYINKETLKYIFTTHFWGPVSNFGIPIAAIYDLKKDPTLISGPMTFALVTYSGVFMKYALSV 77
MPC2 1 ----MSTSSVRFAFRRFWQSETG--PKTVHFWAPTLKWGLVFAGFSDMKRPVEKISGAQNLSLLSTALIWTRWSFVI 71
MPC3 1 ----MSASAFNFAFRRFWNSETG--PKTVHFWAPTLKWGLVFAGLNDIKRPVEKVSGAQNLSLLATALIWTRWSFVI 71
L2-3
transmembrane helix 3
MPC1 78 SPKNYLLFGCHLINETAQLAQGYRFLKYTYFTTDEEKKALDKEWKEKEKTGKQ----- 130
MPC2 72 KPRNILLASVNSFLCLTAGYQLGRIANYRIRNGDSISQLCSYILSGADESKKEITTGR 129
MPC3 72 KPKNYLLASVNFFLGCTAGYHLTRIANFRIRNGDSFKQVIHYIIKGETPAAVAAKQTASTSMNKGVIGTNPPITH 146

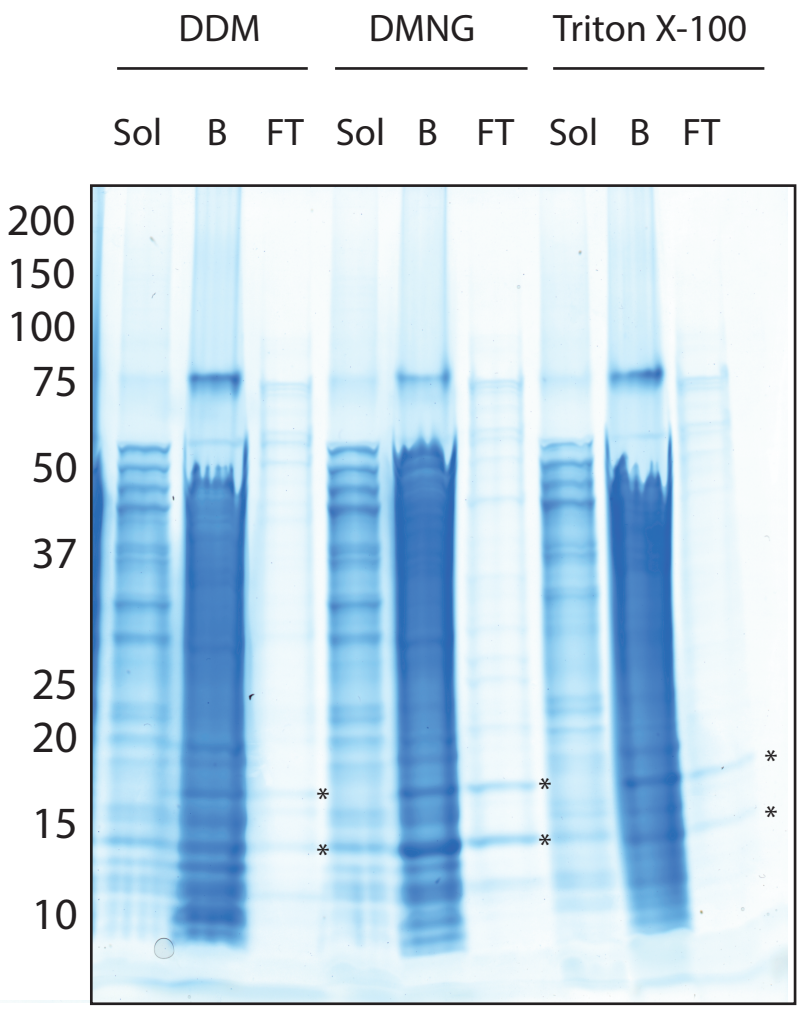
DDM
DMNG
Triton X-100
Sol
B
FT
Sol
B
FT
Sol
B
FT
200
150
100
75
50
37
25
20
15
10
*
*
*
*
*
*

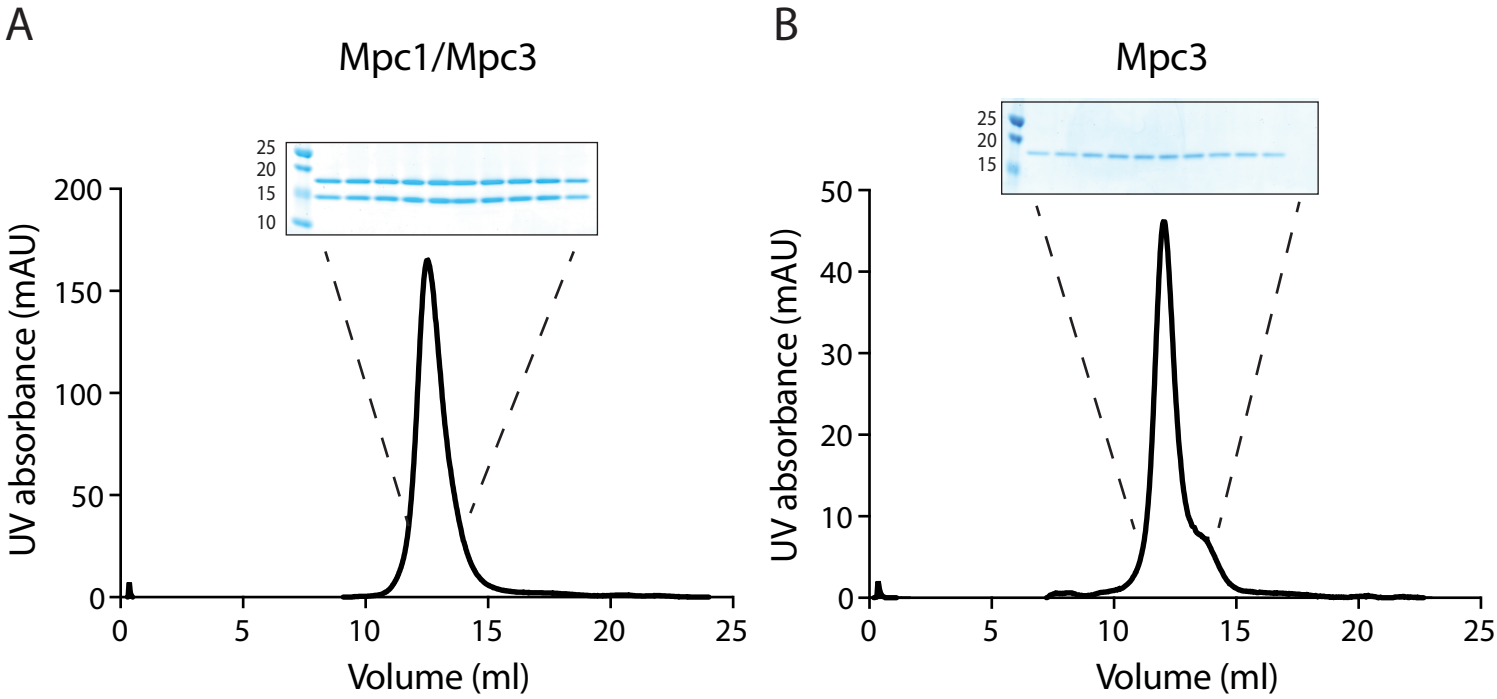
A
Mpc1/Mpc3
25
20
15
10
200
150
100
50
0
UV absorbance (mAU)
0
5
10
15
20
25
Volume (ml)
B
Mpc3
25
20
15
50
40
30
20
10
0
UV absorbance (mAU)
0
5
10
15
20
25
Volume (ml)

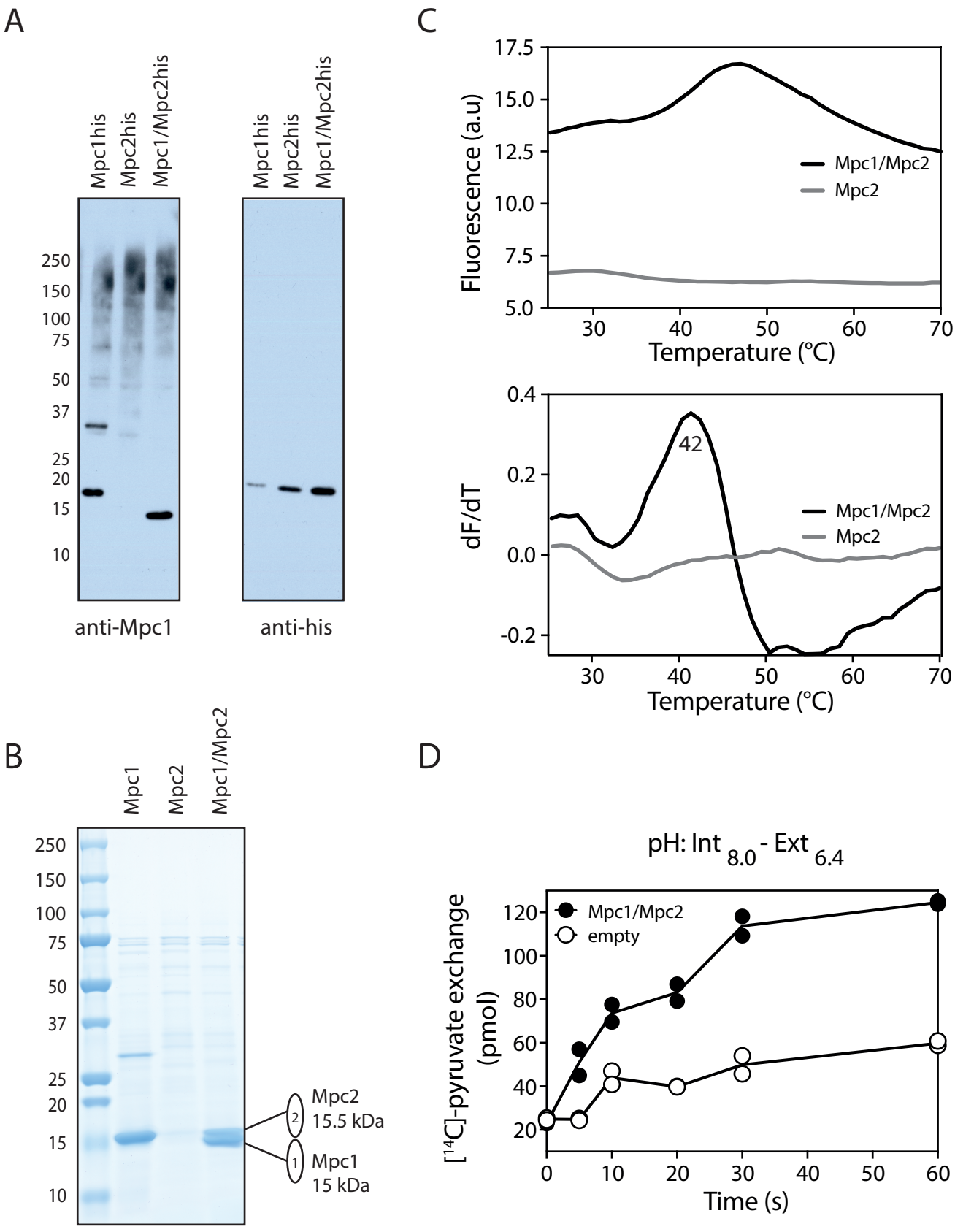
A
Mpc1his
Mpc2his
Mpc1/Mpc2his
250
150
100
75
50
37
25
20
15
10
anti-Mpc1
anti-his
B
Mpc1
Mpc2
Mpc1/Mpc2
Mpc2
15.5 kDa
Mpc1
15 kDa
C
Fluorescence (a.u)
Temperature (°C)
Mpc1/Mpc2
Mpc2
dF/dT
42
D
pH: Int 8.0 - Ext 6.4
[14C]-pyruvate exchange (pmol)
Mpc1/Mpc2
empty
Time (s)

A

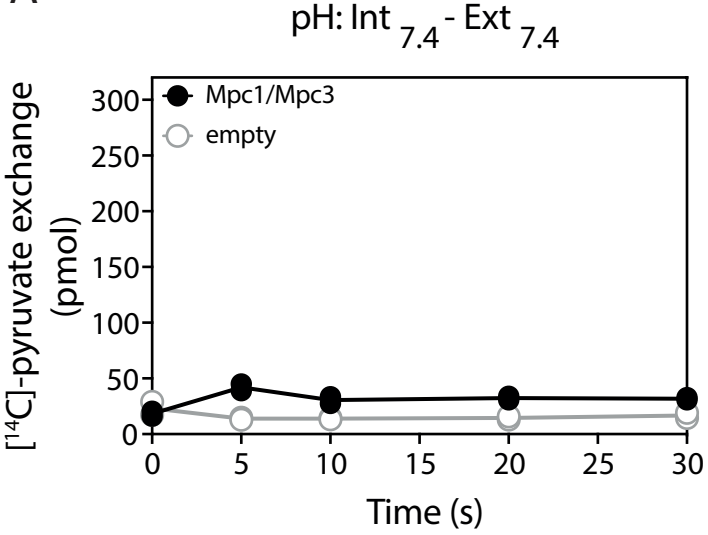
pH: Int 7.4 - Ext 7.4
Mpc1/Mpc3
empty
[14C]-pyruvate exchange (pmol)
300
250
200
150
100
50
0
0
5
10
15
20
25
30
Time (s)

B

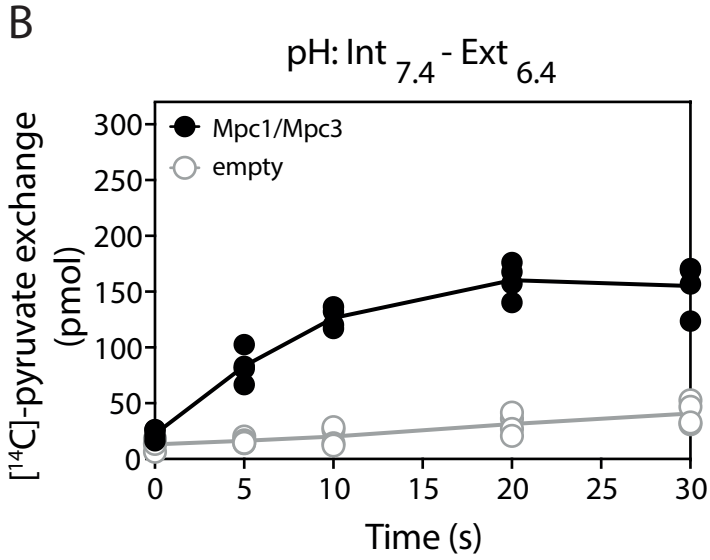
pH: Int 7.4 - Ext 6.4
Mpc1/Mpc3
empty
[14C]-pyruvate exchange (pmol)
300
250
200
150
100
50
0
0
5
10
15
20
25
30
Time (s)

C

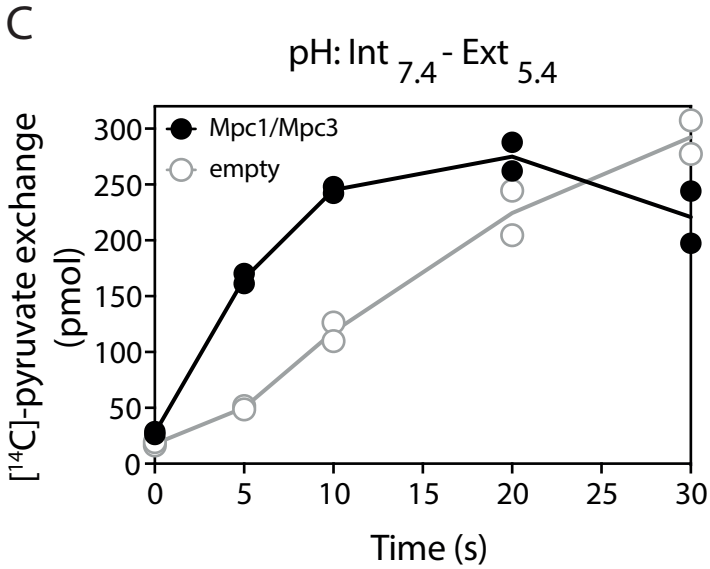
pH: Int 7.4 - Ext 5.4
Mpc1/Mpc3
empty
[14C]-pyruvate exchange (pmol)
300
250
200
150
100
50
0
0
5
10
15
20
25
30
Time (s)